TXNIP in liver sinusoidal endothelial cells ameliorates alcohol-associated liver disease

Eunhye Jung[1,#], Eun Bok Baek[1,#], Eun-Ju Hong[1], Jee Hyun Kang[1], Suyoung Park[1], Eui-Ju Hong[1], Young-Eun Cho[2], Je-Won Ko[1], Young-Suk Won[3,*], and Hyo-Jung Kwon[1,*]

[1]College of Veterinary Medicine, Chungnam National University, Daejeon 34134, Republic of Korea; [2]Andong National University, Andong 36729, Republic of Korea; [3]Laboratory Animal Resource Center, Korea Research Institute of Bioscience and Biotechnology, Chungbuk 28116, Republic of Korea

[#] **These authors contributed equally to this work.**

***Corresponding author**

Hyo-Jung Kwon, DVM, PhD,

Department of Veterinary Pathology, College of Veterinary Medicine, Chungnam National University, 99 Daehak-ro, Yuseong-gu, Daejeon 34134, Korea.

Tel.: 82-42-821-6755; Fax: 82-42-821-8903; E-mail: hyojung@cnu.ac.kr

Young-Suk Won, PhD

Laboratory Animal Resource Center, Korea Research Institute of Bioscience and Biotechnology, Ochang-eup, Cheongwon-gu, Cheongju-si, Chungcheongbuk-do 28116, Korea.

Tel.: 82-43-240-6562; Fax: 82-43-6519; E-mail: yswon@kribb.re.kr

Running title: TXNIP in LSECs protects against ALD

Electronic word count: 167 words (abstract), 8,221 words (including abstract, main text, and main figure legends)

List of abbreviations: ADH, alcohol dehydrogenase; ALD, alcohol-associated liver disease; ALDH2, aldehyde dehydrogenase 2; ALT, aspartate transaminase; AST, alanine transaminase; CYP2E1, cytochrome P450 family 2 subfamily E member 1; CCL4, C-C motif chemokine 4; COL1α1, collagen 1 α1; DEGs, differentially expressed genes; ECs, endothelial cells; eNOS, endothelial nitric oxide synthase; ERK, extracellular signal-regulated kinase; ET-1, endothelin-1; HCC, hepatocellular carcinoma; HSCs, hepatic stellate cells; ICAM-1, intercellular adhesion molecule 1; IL, interleukin; JNK, c-Jun N-terminal kinase; KCs, Kupffer cells; KEGG, Kyoto encyclopedia of genes and genomes; LPS, Lipopolysaccharide; LSECs, liver sinusoidal endothelial cells; LYVE-1, lymphatic vessel endothelial hyaluronan receptor 1; MCP-1, monocyte chemoattractant protein-1; NAFLD, nonalcoholic fatty liver disease; NO, nitric oxide; TAK1, transforming growth factor β-activated kinase 1; TGF-β, transforming growth factor-β; TIMP-1, tissue inhibitor of metalloproteinases-1; TNF-α, tumor necrosis factor-α; TXNIP, thioredoxin interacting protein; α-SMA, alpha-smooth muscle actin; VAP-1, vascular adhesion protein 1, VCAM-1, vascular cell adhesion protein 1; WT, wild-type.

Abstract

Dysregulation of liver sinusoidal endothelial cell (LSEC) differentiation and function has been reported in patients with alcohol-associated liver disease (ALD), but how LSEC alteration contributes to the pathogenesis of ALD remains unclear. Here, we found that the hepatic level of thioredoxin interacting protein (TXNIP) was up-regulated in ALD patients and ethanol diet-fed mice with high expression in LSECs. Notably, endothelial cell-specific *Txnip* deficiency in mice exacerbated alcohol-induced liver injury, inflammation, fibrosis, and hepatocellular carcinoma (HCC) development. Deletion of *Txnip* in LSECs led to sinusoidal capillarization, down-regulation of endothelial nitric oxide synthase (eNOS) level and nitric oxide (NO) production, and increased release of pro-inflammatory cytokines and adhesion molecules. Mechanistically, TXNIP interacted with transforming growth factor β-activated kinase 1 (TAK1) and subsequently suppressed TAK1/c-Jun N-terminal kinase (JNK) pathway. Inhibition of TAK1 activation restored the effect of *Txnip* deficiency on LSECs, thereby blocking ethanol-induced liver injury and inflammation. Overall, TXNIP in LSECs protects against ALD progression through TAK1/JNK signaling and TXNIP targeting may be a potential therapeutic approach for ALD.

Keywords: Alcohol-associated liver disease/JNK/Liver sinusoidal endothelial cells/TAK1/ TXNIP

Introduction

Alcohol-associated liver disease (ALD) is a major cause of chronic liver disease, affecting millions of patients worldwide. The pathological process of disease development involves early steatosis and steatohepatitis, with some individuals ultimately progressing to fibrosis/cirrhosis and even hepatocellular carcinoma (HCC) (Gao & Bataller, 2011; Osna *et al*, 2017). Disease progression and pathogenesis are relatively well understood, but the exact mechanisms underpinning ALD pathogenesis remain unclear and there is currently no accepted therapy to prevent or cure the disease.

Liver sinusoidal endothelial cells (LSECs) are specialized endothelial cells (ECs) that line liver sinusoids. These highly endocytic ECs exhibit a characteristic phenotype of nondiaphramed fenestrae and the lack of basal membrane, which facilitates highly efficient material exchange between blood and the space of Disse (Gracia-Sancho *et al*, 2021; Hammoutene & Rautou, 2019; Poisson *et al*, 2017). Normally, LSECs increase nitric oxide (NO) production under shear stress in hepatic sinusoids to regulate blood flow and maintain their differentiated phenotype in an autocrine fashion. Meanwhile, healthy differentiated LSECs maintain Kupffer cells (KCs) and hepatic stellate cells (HSCs) in the quiescent state through endothelial NO synthase (eNOS)-dependent NO pathways. Under pathological conditions, LSECs dedifferentiate to a state called capillarization. Capillarized LSECs lose their fenestrae and express extracellular matrix (ECM) to develop a basement membrane. This results in LSEC dysfunction, which contributes to KCs and HSCs activations and hepatocyte damage. Altered LSECs also release pro-inflammatory mediators and overexpress adhesion molecules, which in turn promotes liver inflammation and fibrosis (Gracia-Sancho *et al.*, 2021; Hammoutene & Rautou, 2019; Poisson *et al.*, 2017). Although LSEC capillarization and dysfunction are recognized as initial pathological markers in various liver

diseases, including ALD (Mak *et al*, 2022; McCuskey *et al*, 2005), the mechanisms involved in the impact of LSECs on the development of ALD remain unclear.

Thioredoxin-interacting protein (TXNIP) is a stress-response gene that is also called thioredoxin-binding protein-2 (TBP-2) or vitamin D upregulated protein 1 (VDUP1) (Pan *et al*, 2022). TXNIP can induce oxidative damage by binding to thioredoxin (TRX) and inhibiting its antioxidant activity (Junn *et al*, 2000; Nishiyama *et al*, 1999). TXNIP is linked to physiological processes related to cell growth, cell survival, and the pathogeneses of various diseases (Mohamed *et al*, 2021; Pan *et al.*, 2022). In the liver, TXNIP is significantly up-regulated in nonalcoholic fatty liver disease (NAFLD) patients and mediates lipogenesis and fatty acid re-esterification (Donnelly *et al*, 2004; Park *et al*, 2014). Our previous study has also demonstrated that TXNIP is upregulated in NAFLD patients and elevated TXNIP attenuated steatohepatitis via autophagy and fatty acid oxidation (Park *et al*, 2021). In addition, TXNIP expression is suppressed in human HCC tissues, and TXNIP negatively regulates hepatocarcinogenesis by suppressing TNF-α-induced NF-kB activation (Kwon *et al*, 2010).

Recently, TXNIP was shown to mediate EC inflammation in response to disturbed blood flow by increasing monocyte adhesion (Wang *et al*, 2012). It also triggers early apoptosis in high-glucose-treated human aortic endothelial cells (HAECs) (Li *et al*, 2017; Li *et al*, 2009) and its up-regulated expression contributes to oxidative stress and endothelial dysfunction in hypertensive rats (Li *et al.*, 2017; Wang *et al*, 2022). Furthermore, TXNIP can suppress eNOS activity and disrupt NO signaling (Huan *et al*, 2017; Schulze *et al*, 2006), suggesting that it may negatively regulate endothelial function. However, little is known about the role of TXNIP in LSECs during liver diseases development. Here, we show that alcohol exposure increases TXNIP expression in LSECs. Using mice genetically lacking

Txnip in LSECs and a human LSEC line, we demonstrate that TXNIP regulates LSEC phenotype and function by interacting with transforming growth factor β-activated kinase 1 (TAK1) and the c-Jun N-terminal kinase (JNK) pathway, which protects against ALD development.

Results

TXNIP expression is up-regulated in the livers of ALD patients and EtOH-diet fed mice

To analyze whether TXNIP expression is associated with ALD development, we first examined the hepatic levels of TXNIP in patients with ALD. Immunohistochemistry (IHC) revealed markedly increased TXNIP expression in patients with alcohol-associated steatosis and fibrosis compared with healthy controls (Fig 1A). The degree of TXNIP expression was positively related with the macro-fat % and fibrosis grade (Fig 1B and C). Correlative analysis also found a significant association between increased TXNIP expression and ethanol intake amount in alcoholic patients with fibrosis but not steatosis (Fig 1B and C). Consistent with the findings in human samples, TXNIP protein and mRNA expression levels were significantly increased in mice fed an EtOH-diet (Fig 1D and E). Taken together, these data suggest that TXNIP overexpression is related to ALD and TXNIP might play an important role in this process.

Txnip deficient mice are more susceptible to ethanol-induced liver injury, inflammation, fibrosis, and HCC development

To investigate how TXNIP contributes to ALD development, *Txnip* total knockout (*Txnip*$^{-/-}$) and wild-type (WT) mice were fed a control or 4% ethanol diet for 1 year. Ethanol-fed *Txnip*$^{-/-}$ mice had a lower survival rate, higher liver-to-body weight ratios, and higher serum levels of aspartate transaminase (ALT) and alanine transaminase (AST) than ethanol-fed WT mice (Fig 2A and B, Appendix Fig S1A). Strikingly, we found that 3 of 9 ethanol-fed *Txnip*$^{-/-}$ mice (33.3%) developed tumor nodules of variable size in the liver, whereas no obvious hepatic tumor was observed in ethanol-fed WT mice (Fig 2C-E).

Chronic liver inflammation and the resultant fibrotic/cirrhotic microenvironment promote the initiation and progression of HCC (Hernandez-Gea *et al*, 2013). Hematoxylin and eosin (H&E) and Oil Red O staining revealed that ethanol-fed *Txnip*$^{-/-}$ mice had a higher degree of steatosis than ethanol-fed WT mice (Fig 2F, Appendix Fig S1B). In addition, ethanol-fed *Txnip*$^{-/-}$ mice exhibited increased hepatic level of triglyceride (TG), number of F4/80- and myeloperoxidase (MPO)-positive cells, and Sirius red-positive area (Fig 2F, Appendix Fig S1C). Quantitative real-time PCR (qRT-PCR) showed that the hepatic levels of genes involved in inflammation (tumor necrosis factor (TNF)-α and monocyte chemoattractant protein-1 (MCP-1)) and fibrosis (transforming growth factor (TGF)-β, collagen 1 α1 (COL1α1), and tissue inhibitor of metalloproteinases (TIMP)-1) were markedly elevated in *Txnip*$^{-/-}$ mice (Appendix Fig S1D and E). Next, we determined the effects of TXNIP on short-term ethanol exposure. *Txnip*$^{-/-}$ mice exhibited a higher liver-to-body weight ratio and greater levels liver injury (serum ALT and ALT levels), steatosis (H&E staining and TG levels), oxidative stress (malondialdehyde (MDA) and total glutathione levels), and inflammation (F4/80, TNF-α, interleukin (IL)-6, IL-1β, and MCP-1 expression levels) after 4 weeks of alcohol feeding (Appendix Fig S2). These results suggest that *Txnip* deficiency exacerbates alcohol-associated hepatic inflammation and fibrosis to provide a favorable microenvironment for HCC development.

Endothelial-specific deletion of Txnip exacerbates ethanol-induced liver tumorigenesis

Because TXNIP was up-regulated in ALD patients and ethanol-fed mice, we investigated which cell types were responsible for this effect. Hepatocytes, HSCs, KCs, and LSECs were isolated from chronic-binge ethanol-fed WT mice, and TXNIP expression was analyzed. In control diet-fed WT mice, the major TXNIP-expressing cell was LSECs, which

exhibited approximately 11.5-fold and 7.49-fold higher levels, respectively, than hepatocytes and KCs (Fig 3A). Chronic-binge ethanol feeding increased *TXNIP* mRNA levels in KCs (1.4-fold) and LSECs (1.8-fold), but not hepatocytes (Fig 3A). We also co-stained liver sections for TXNIP and markers of KCs (F4/80) or LSECs (lymphatic vessel endothelial hyaluronan receptor 1; LYVE-1) and found that TXNIP was highly expressed in KCs and LSECs (Fig 3B).

To determine which hepatic cell type contributed to alcohol-induced liver diseases by expressing TXNIP, we generated macrophage- or EC-specific *Txnip*-deficient ($Txnip^{\Delta Mac}$ and $Txnip^{\Delta EC}$) mice by crossing $Txnip^{fl/fl}$ mice with *LysM-Cre* and *Tie2-Cre* transgenic mice, respectively. Loss of *Txnip* expression was confirmed by a nondetectable *Txnip* mRNA levels in KCs and LSECs isolated from of $Txnip^{\Delta Mac}$ or $Txnip^{\Delta EC}$ mice compared with control ($Txnip^{fl/fl}$) mice (Fig 3C). We then determined the effect of KCs or LSECs *Txnip* depletion on ALD development. Compared with $Txnip^{fl/fl}$ mice, $Txnip^{\Delta EC}$ mice had higher levels of serum ALT and AST, hepatic TNF-α, IL-6, IL-1β, and F4/80 expressions, and MDA after 4 weeks of alcohol feeding, but a lower total glutathione level after ethanol feeding; meanwhile there was no significant difference in hepatic TG or cholesterol (Fig 3D-G). $Txnip^{\Delta Mac}$ mice showed no significant change in liver injury or inflammatory response, but exhibited higher oxidative stress than $Txnip^{fl/fl}$ mice (Fig 3D-G).

We further examined whether the increased liver injury and inflammation in $Txnip^{\Delta EC}$ mice were associated with HCC development. After 1 year ethanol feeding, hepatic tumorigenesis was strongly accelerated in $Txnip^{\Delta EC}$ mice compared with $Txnip^{fl/fl}$ mice (Fig 3H and I) and was associated with increased liver damage (serum ALT and AST levels and liver histology), inflammation (IL-6, MCP-1, C-C motif chemokine 4; CCL4, vascular cell adhesion molecule 1; VCAM-1, and vascular adhesion protein 1; VAP-1), and fibrosis

(laminin, COL1α1, COL3α1, and COL4α1) (Fig 3J, Appendix Fig S3). These results indicate that endothelium-specific deletion of *Txnip* is likely to increase the susceptibility to ethanol-induced inflammation, fibrosis, and HCC development.

Endothelial Txnip deficiency promotes LSEC capillarization, dysfunction, and pro-inflammatory phenotype

To evaluate the effects of TXNIP on LSECs, we performed RNA-seq on LSECs isolated from *Txnip*$^{-/-}$ and WT mice (Appendix Fig S4A). The two groups could be clearly separated by cluster analysis, indicating that they differed significantly (Appendix Fig S4B). Gene set enrichment analysis (GSEA) revealed that cellular signaling pathways or genes related to inflammation, angiogenesis, and vasculature morphogenesis/development were significantly affected by *Txnip* deficiency (Fig 4A). A heatmap revealed that *Txnip*-deficient LSECs showed down-regulation of LSEC-associated genes but up-regulation of capillary EC-associated genes (Appendix Fig S4C). qRT-PCR confirmed that the capillary EC markers, endothelin-1 (ET-1) and CD34, were up-regulated in *Txnip*-deficient LSECs, whereas the LSEC differentiation markers, stabilin-1 (stab1) and stabilin-2 (stab2), were reduced (Fig 4B). Lipopolysaccharide (LPS) treatment promoted LSEC capillarization, which was much greater in *Txnip*-deficient LSECs (Fig. 4B). To directly determine the role of TXNIP in LSECs, we established a stable TXNIP-overexpressed (TXNIP-OE) human LSEC line and found that TXNIP overexpression suppressed LSEC capillarization under a normal culture condition and after LPS challenge (Appendix Fig S5A). Consistently, 1 year of ethanol feeding significantly decreased LSEC-associated protein (LYVE-1) expression in *Txnip*$^{\Delta EC}$ mice but increased the protein and mRNA levels of capillary EC-related factors (CD31, CD34, and ET-1) (Fig 4C, Appendix Fig S5B). The eNOS-NO signaling pathway maintains

the LSEC differentiated phenotype, and dysfunctional LSECs exhibit impaired NO production (Yang *et al*, 2021). The protein expression of phospho-eNOS, the mRNA level of eNOS, and NO production were lower in *Txnip*-deficient LSECs than in WT LSECs under a normal culture condition and after LPS treatment (Fig 4D-F), but opposite results were observed in TXNIP-OE TMNK-1 cells (Appendix Fig S6A and B). Furthermore, 1 year ethanol-fed $Txnip^{\Delta EC}$ mice showed significantly decreased expressions of eNOS versus $Txnip^{fl/fl}$ mice (Appendix Fig S6C).

Capillarized and dysfunctional LSECs acquire a pro-inflammatory phenotype and function via pro-inflammatory mediators release and adhesion molecules overexpression (Hammoutene & Rautou, 2019). Analysis of RNA-seq data indicated that a set of genes involved in inflammation was changed upon *Txnip* knockout (Appendix Fig S7A). Consistently, *Txnip*-deficient LSECs showed up-regulation of TNF-α, IL-6, IL-1β, MCP-1, CCL4, and VCAM-1 versus WT LSECs after LPS treatment (Fig 4G). In addition, LSECs isolated from chronic-binge ethanol-fed $Txnip^{\Delta EC}$ mice exhibited increased levels of TNF-α, IL-6, IL-1β, and MCP-1 (Appendix Fig S7B). These results collectively suggest that lack of endothelial *Txnip* results in altered LSEC phenotype and function, which might promote liver injury and inflammation.

Endothelial Txnip regulates alcohol metabolism in LSECs

To investigate the mechanism by which TXNIP regulates LSECs, we searched for differentially expressed genes (DEGs) by analyzing RNA-seq data from LSECs of $Txnip^{-/-}$ and WT mice. We obtained 326 DEGs, 139 up-regulated and 187 down-regulated, in *Txnip*-deficient versus WT LSECs (Fig 5A). Kyoto Encyclopedia of Genes and Genomes (KEGG) pathway enrichment analysis showed that the ALD-related pathway such as alcohol

metabolism was the most significantly changed by *Txnip* deficiency (Fig 5B, Appendix Fig S8). Alcohol dehydrogenase 1 (ADH1) and cytochrome P450 family 2 subfamily E member 1 (CYP2E1) are the main enzymes for oxidizing ethanol to acetaldehyde, while aldehyde dehydrogenase 2 (ALDH2) converts acetaldehyde to acetate (Zakhari, 2006). CYP2E1 and ADH1 are constitutively expressed in LSECs (Yang *et al.*, 2021). Thus, we examined whether the accelerated HCC development in $Txnip^{\Delta EC}$ mice was associated with altered alcohol metabolism in LSECs. Indeed, *Txnip*-deficient LSECs exhibited increased ADH and reduced ALDH activities after ethanol treatment, while TXNIP-OE TMNK-1 cells showed decreased ADH and elevated ALDH activities (Fig 5C, Appendix Fig S9A). Alcohol treatment increased CYP2E1 protein levels in LSECs, but *Txnip* deficiency or overexpression did not affect this parameter (Fig 5D, Appendix Fig S9B). We further examined whether altered alcohol metabolizing enzyme activity in *Txnip*-deficient LSECs affects ethanol-induced HCC development *in vivo*. As shown Fig 5E, there was no difference in the protein levels of CYP2E1, ADH, and ALDH1/2 between $Txnip^{fl/fl}$ and $Txnip^{\Delta EC}$ mice after alcohol gavage. We also determined the blood acetaldehyde and acetate concentrations and found no difference between $Txnip^{fl/fl}$ and $Txnip^{\Delta EC}$ mice (Fig 5F). These results indicate that TXNIP regulates activity of alcohol metabolic enzymes in LSECs, but this effect is not sufficient to promote alcohol-induced HCC development in $Txnip^{\Delta EC}$ mice.

TXNIP interacts with TAK1 and regulates TAK1/JNK signaling in LSECs

Considering RNA-seq results showing mitogen-activated protein kinase (MAPK) pathway was one of the most significantly changed by *Txnip* deficiency (Fig 5B), we explored the activation of MAPK signaling in LSECs. LPS treatment elevated TAK1 and JNK phosphorylation, and these changes were greatly increased and decreased in *Txnip*-

deficient and -OE LSECs, respectively (Fig 6A and B). TAK1 and JNK activations were also increased in ethanol-fed *Txnip*$^{\Delta EC}$ mice versus *Txnip*$^{fl/fl}$ mice (Fig 6C). *Txnip* deficiency or overexpression in LSECs affected the phosphorylations of p38 MAPK and extracellular signal-regulated kinase (ERK) *in vitro*, but these signals were not changed in ethanol-fed *Txnip*$^{\Delta EC}$ mice (Appendix Fig S10). To further examine the potential molecular mechanism by which TXNIP regulates the MAPK pathway in LSECs, we detected the localizations of TXNIP and TAK1. Immunofluorescence (IF) staining showed that TXNIP co-localized with TAK1 in the cytoplasm of TMNK1 cells (Fig 6D). Co-immunoprecipitation (IP) experiments revealed that TXNIP interacted with TAK1 in TMNK-1 cells (Fig 6E). Taken together, these data demonstrate that TXNIP interacts with TAK1 and inhibitsTAK1/JNK pathway in LSECs.

Inhibition of TAK1 activity blocks ethanol-induced liver injury and inflammation in Txnip$^{\Delta EC}$ mice

To further clarify whether TAK1 mediates the effects of TXNIP on ALD development, TAK1 activity was blocked in LSECs using a specific TAK1 inhibitor. Compared with a vehicle control group, NG25 treatment suppressed the LPS-induced phosphorylation of TAK1 and JNK in *Txnip*-deficient LSECs (Fig 7A). In addition, NG25 reversed the down-regulation of eNOS and up-regulation of pro-inflammatory mediators and VCAM-1 in LPS-treated *Txnip*-deficient LSECs (Fig 7B and C). The requirement of TAK1 for TXNIP function was further validated by *in vivo* experiments. *Txnip*$^{fl/fl}$ and *Txnip*$^{\Delta EC}$ mice were fed an ethanol diet accompanied with NG25. Ethanol-diet induced increases in liver injury (liver histology and serum ALT and AST levels), oxidative stress (MDA), and cytokines and adhesion molecule levels (TNF-α, IL-6, IL-1β, MCP-1, CCL4, and VCAM-1) in *Txnip*$^{\Delta EC}$ mice were reduced to levels similar to those in *Txnip*$^{fl/fl}$ mice (Fig 7D-G).

Collectively, these results indicate that TAK1 mediates the protective effect of TXNIP during ALD development.

LSEC capillarization is increased in patients with ALD and positively correlated with TXNIP expression

Finally, we examined the relevance of our experimental findings in ALD patients. Consistent with previous reports (Mak *et al.*, 2022; Urashima *et al*, 1993), the positive area of LYVE-1, a LSEC differentiation marker, was reduced in livers of alcoholic patients with fibrosis compared with normal controls, whereas the positive area of CD31, capillary EC marker, was significantly increased (Fig 8A and B). LYVE-1 expression was negatively correlated with fibrosis grade and ethanol intake amount, while CD31 expression was positively correlated with these parameters (Fig 8C and D).

Similar to our in *vivo* and *in vitro* results, co-IF staining showed TXNIP was co-expressed with LYVE-1 in normal controls, but alcoholic fibrosis patients exhibited co-localization of TXNIP and CD-31 (Fig 8E). Notably, IHC staining revealed strong immune positivity for TXNIP in LSECs of alcoholic fibrosis patients, but weak staining in normal controls (Fig 8F). Examining the correlation between TXNIP and LYVE-1 or CD31 in ALD tissues showed that TXNIP expression was negatively and positively correlated with LYVE-1 and CD31 positive area, respectively, in human subjects (Fig 8G).

Discussion

We show here that TXNIP is up-regulated in the livers of ALD patients compared to healthy controls and those of mice subjected to ethanol feeding. TXNIP is overexpressed mainly in LSECs and mice genetically lacking *Txnip* in ECs exhibit accelerated liver injury, steatohepatitis, fibrosis, and HCC development following ethanol feeding. The increased risk of alcohol-induced hepatocarcinogenesis in $Txnip^{\Delta EC}$ mice is likely due to LSEC capillarization, dysfunction, and pro-inflammatory phenotype. Further experiments show that TXNIP interacts with TAK1, ultimately suppressing TAK1 activation and downstream JNK signaling. Inhibition of TAK1 activation blocks the detrimental effects of *Txnip* knockdown in LSECs on eNOS signaling and pro-inflammatory function, further contributing to decreased liver injury and inflammation in ethanol-fed $Txnip^{\Delta EC}$ mice.

In recent years, numerous publications have implicated altered LSEC phenotype and function in ALD. Biopsy specimens of alcoholics show significantly fewer fenestrations and lower endothelial porosity compared to non-alcoholics, indicating that the sinusoids undergo capillarization early during alcoholic liver injury (Mak *et al.*, 2022; Urashima *et al.*, 1993). Sinusoidal capillarization is also observed in liver biopsies of alcoholic patients with mild fibrosis and increases as fibrosis progress to cirrhosis (Urashima *et al.*, 1993). Here, we found greater LSEC capillarization in ALD patients with fibrosis compared to healthy controls. Increased expression of capillary EC markers in human ALD was correlated with elevated TXNIP expression, providing clinical evidence for a positive relationship between TXNIP up-regulation and LSEC alteration. The contribution of TXNIP to ECs has been reported previously. TXNIP overexpression reduces eNOS phosphorylation and NO generation to impair endothelial function, whereas its knockdown rescues endothelial dysfunction by restoring eNOS expression (Huan *et al.*, 2017; Schulze *et al.*, 2006). TXNIP promotes

inflammation by increasing monocyte adhesion in ECs (Wang *et al.*, 2012), while silencing of TXNIP prevents LPS-induced inflammatory response, apoptosis, and oxidative damage (Hou *et al*, 2019). In contrast, we herein found that *Txnip* deletion in LSECs induced capillarization, reduced the eNOS level and NO production, and increased pro-inflammatory mediator and adhesion molecule release, which were accompanied by accelerated alcohol-induced hepatocarcinogenesis. This discrepancy may be attributed to the unique phenotype of LSECs, which differ morphologically and functionally from capillary ECs due to the presence of typical fenestrations, clustered in sieve plates, and absence of a basement membrane (Hammoutene & Rautou, 2019). Our study clearly shows that TXNIP expression is essential for maintaining LSEC phenotype and function, which is beneficial for decreasing ALD.

Although the mechanisms that trigger LSEC alteration in ALD are not well known, several mediators are potential candidates, including alcohol metabolites, gut-derived LPS, and liver injury (Hammoutene & Rautou, 2019). Another interesting finding from the current study is that TXNIP regulates ethanol metabolizing enzymes in LSECs. Because alcohol is oxidized to acetaldehyde principally in hepatocytes by ADH1, CYP2E1, and catalase, the mechanism of ALD has been largely investigated in parenchymal hepatocytes (Zakhari, 2006). Unlike hepatocytes, LSECs are directly exposed to high concentrations of ethanol. Thus, LSECs could play an important role in ethanol-induced damage through endothelial barrier function derangement (Hammoutene & Rautou, 2019; Poisson *et al.*, 2017). However, a recent study revealed that alcohol metabolism by CYP2E1 in LSECs could contribute to decreased eNOS-derived NO production and increased LSEC dysfunction, leading to alcohol-induced liver injury (Yang *et al.*, 2021). Here, although *Txnip* deficiency altered the activities of ADH and ALDH in LSECs, ethanol-fed $Txnip^{\Delta EC}$ and $Txnip^{fl/fl}$ mice exhibited

similar hepatic levels of CYP2E1, ADH, and ALDH1/2 and blood concentrations of acetaldehyde and acetate. These results suggest that *Txnip* deficiency led to altered alcohol metabolism in LSECs, which is insufficient to affect whole-liver alcohol metabolism, but can contribute to LSEC dysfunction and liver injury. Further study is needed to investigate how TXNIP regulates ethanol metabolizing enzymes in LSECs.

Our systematic RNA-seq analyses further showed that MAPK signaling cascade was closely associated with *Txnip* loss in LSECs. *Txnip* deficiency in LSECs increased JNK activation, which was accompanied by decreased eNOS level and NO production and enhanced inflammatory response. Consistently, JNK phosphorylation was higher in ethanol-fed $Txnip^{\Delta EC}$ versus $Txnip^{fl/fl}$ mice. The activations of p38 MAPK and ERK were not changed in ethanol-fed $Txnip^{\Delta EC}$ mice, indicating that TXNIP protected against hepatic ALD by regulating JNK signals. Previous studies demonstrated that JNK activation contributes to endothelial dysfunction by inhibiting eNOS phosphorylation (Huang *et al*, 2012; Pham *et al*, 2019), whereas JNK inhibition restores eNOS synthase activation and endothelial function (Breton-Romero *et al*, 2016). JNK activation also up-regulates inflammatory mediators and adhesion molecules to promote inflammatory liver diseases development (Das *et al*, 2009; Kodama *et al*, 2009; Schattenberg *et al*, 2006). In addition, preclinical studies on the use of JNK-specific inhibitors have been found to exert protective effects by attenuating endothelial dysfunction and inflammation (Hein *et al*, 2019; Liu *et al*, 2014). We further explored the direct interaction of MAPK pathway with TXNIP and found that TXNIP interacts with TAK1 and regulates its activation in LSECs. A previous study showed that TXNIP interacted with the 35–291 region of TAK1 in HEK 293 cells and inhibited TAK1 activity by interfering with formation of the TAK1 and TAK1-binding protein 1 (TAB1) complex (Kim *et al*, 2020). Although how TXNIP regulates TAK1 in LSECs still needs to be further studied, our results

show that TXNIP interacts with TAK1, thus attenuating TAK1 phosphorylation and subsequent JNK signaling in LSECs. The potential role of TAK1 in various liver diseases, including ischemia-reperfusion injury, NAFLD, NASH, and HCC, has been well defined (Inokuchi *et al*, 2010; Qian *et al*, 2022; Tan *et al*, 2020; Zhang *et al*, 2022). Suppression of TAK1 and its downstream signaling significantly promotes liver injury, inflammation, fibrosis, and tumor formation (Inokuchi *et al.*, 2010; Tan *et al.*, 2020). TAK1 hyperactivation, on the other hand, induces hepatic steatosis, inflammation, and fibrosis, whereas TAK1 activity suppression alleviates the progression of these diseases (Inokuchi *et al.*, 2010; Mahata *et al*, 2021; Qian *et al.*, 2022; Zhang *et al.*, 2022). Here, TAK1 inhibition attenuated JNK activation, restored the eNOS level, and down-regulated cytokines and adhesion molecule in *Txnip*-deficient LSECs. Furthermore, ethanol-induced liver injury and inflammation were ameliorated in $Txnip^{\Delta EC}$ mice following TAK1 inhibitor treatment. These results demonstrate that TXNIP plays a protective role in ALD by suppressing the TAK1 activation and downstream JNK signaling.

Conservation of the LSEC phenotype and prevention of capillarization may reduce the risk of progressing from inflammation and fibrosis to irreversible cirrhosis and HCC (Wilkinson *et al*, 2020). Approaches that maintain LSEC differentiation and function include restoration of their fenestrated phenotype via bone morphogenic protein 9 (BMP9) and GATA4 (Desroches-Castan *et al*, 2019; Geraud *et al*, 2017), reconstitution of VEGF/NO/sGC signaling (Marrone *et al*, 2013; Tateya *et al*, 2011; Xie *et al*, 2012), and reestablishment of normal hedgehog signaling (Zhao *et al*, 2017). The current study shows that TXNIP maintains LSEC phenotype and function through interactions with TAK1 and JNK signaling, which protects against ALD progression. Our findings provide insights into LSEC-mediated

ALD development and suggest that targeting TXNIP may be a potential strategy to confer protection against ALD.

Materials and Methods

Human liver samples

Tissue microarrays containing specimens of ALD were purchased from SEKISUI XenoTech (Kansas City, KC, USA). Each tissue microarray contained 13 samples of normal human liver (#TMA.NORM) without a history of alcohol consumption and 19 and 18 samples of steatosis (#TMA.AS) and fibrosis (#TMA.FIB) with a history of alcohol use, respectively. The general characteristics of normal and ALD human liver samples are listed in Appendix Table S1. The human study was approved by the Chungnam National University Institutional Review Board (Approval Number: 02205-BR-061-01) in accordance with the Declaration of Helsinki and the principles set out in the Department of Health and Human Services Belmont Report.

Animal experiments

Txnip$^{-/-}$ mice on a C57BL/6J background were as described previously (Park *et al.*, 2021) and C57BL/6J mice were used as controls. Macrophage- or EC-specific *Txnip*-deficient (*Txnip*$^{\Delta Mac}$ and *Txnip*$^{\Delta EC}$) mice were generated by crossing *Txnip*$^{fl/fl}$ mice (The Jackson Laboratory, Bar Harbor, ME, USA) with *LysM-Cre* and *Tie2-Cre* transgenic mice (The Jackson Laboratory), respectively. Animals were maintained on a standard rodent chow diet and a 12-h light/dark cycle. All animal studies were approved by the Chungnam National University Animal Care and Use Committee (Approval Number: 202103A-CNU-093 and 202203A-CNU-012) and conducted in accordance with the principles and procedures outlined in the National Institutes of Health (NIH) Guide for the Care and Use of Laboratory Animals.

Mouse models for ethanol consumption

Eight-week-old female or male *Txnip*$^{-/-}$, *Txnip*$^{\Delta Mac}$, *Txnip*$^{\Delta EC}$, *Txnip*$^{fl/fl}$, and wild-type (WT) mice were fed either Lieber–DeCarli liquid diet containing 4 or 5% ethanol (EtOH-fed) or liquid control diet (pair-fed) for 1 year or 4 weeks. In detail, mice were initially fed with Lieber-DeCarli diet (Dyets, Bethlehem, CA, USA) *ad libitum* for 5 days to adapt to a liquid diet, and then with a gradual increase of the ethanol (Sigma-Aldrich, St. Louis, MO, USA) content by 1% (v/v) each day until it reached 4% or 5% (v/v). Then, the mice were kept on this liquid diet for a total of 1 year (4%) or 4 weeks (5%). Diet intake amount was measured daily. In some experiments, mice were fed with 5% ethanol for 10 days followed by one EtOH binge (5 g/kg, referred to as the chronic-binge model), as described previously (Bertola *et al*, 2013). For NG25 treatment, *Txnip*$^{\Delta EC}$ and *Txnip*$^{fl/fl}$ mice were fed a liquid diet containing 5% ethanol diet for 4 weeks with further administration of NG25 (5 mg/kg/day intraperitoneally; cat# S8868, MedChemExpress, Monmouth Junction, NJ, USA) or vehicle.

Blood chemistry and hepatic lipid levels

Serum ALT, AST, cholesterol, and triglyceride levels were determined using a HITACHI 7020 chemistry analyzer (Hitachi, Tokyo, Japan). Hepatic cholesterol and triglyceride content were determined using a cholesterol quantitation kit (cat# K623-100, BioVision, Waltham, MA, USA) and a triglyceride colorimetric assay kit (cat# 10010303, Cayman, Ann Arbor, MI, USA), respectively.

Histological examination

Formalin-fixed liver samples were paraffin embedded, sectioned (4-μm-thick), and stained with H&E (cat# 081313-500 and 052501-500, Labcore, Seoul, Korea). Fat accumulation in

the liver was analyzed in 10-μm-thick frozen sections with Oil Red O solution staining (cat# O1516, Sigma-Aldrich), Mayer's hematoxylin (cat# 081313-500, Labcore) counterstaining, and light microscopic analysis (Nikon, Tokyo, Japan). For analysis of collagen deposition in liver tissues, paraffin sections were stained with Sirius red (cat# IW-3012, IHC World, Woodstock, MD, USA) counterstained with Mayer's hematoxylin, and analyzed via light microscopy. The positive area was calculated from at least five magnification (×400) fields per liver section.

IHC analysis

Paraffin-embedded liver tissues from human and mice were used for IHC analyses. Tissues were incubated with primary antibody against TXNIP (cat# ab188865, Abcam, Cambridge, United Kingdom), F4/80 (cat# ab6640, Abcam), MPO (cat# ab9535, Abcam), CD31 (cat# ab28364, Abcam), or LYVE1 (cat# AF2089, R&D Systems, Minneapolis, MN, USA) and the corresponding biotinylated secondary antibodies and the ABC tertiary reagent (cat# PK-6101 and PK-6104, VECTASTAIN ABC Kit; Vector Laboratories) was employed to amplify the signal. IHC results were developed with 3,3'-diaminobenzidine (DAB; cat# SK-4100, Vector Laboratories). The slides were counterstained with Mayer's hematoxylin, dehydrated, and mounted with mounting medium (cat# 9990440, Mercedes Scientific, Lakewood Ranch, FL, USA). For analysis of TXNIP expression, five fields (final magnification, ×200) were randomly selected for each slide, and the integrated optical density (IOD) of all positive staining in each image was measured. F4/80- or MPO-positive cells were counted in 10 randomly selected fields per section (final magnification, ×400).

IF analysis

Human and mouse liver sections were incubated with primary antibodies against TXNIP (cat# ab188865, Abcam), F4/80 (cat# ab6640, Abcam), CD31 (cat# ab28364 and ab56299, Abcam), or LYVE1 (cat# AF2089 and BAF2125, R&D Systems) and fluorescence-conjugated antibodies (cat# A32731, A32816, and A21424, Invitrogen, Waltham, MA, USA). All samples were mounted with Fluoroshield™ containing 4′,6-diamidino-2-phenylindole (DAPI; cat# P36935, Invitrogen), and observed by a confocal microscope (LSM 880; Carl Zeiss, Oberkochen, Germany). The LYVE-1- or CD31-positive area was analyzed in 10 randomly selected fields per section (final magnification, ×400).

RNA isolation and qRT-PCR

Total RNA was extracted from mouse liver tissues and cells using TRIzol (cat# 15596018, Thermo Fisher Scientific, Waltham, MA, USA) according to the manufacturer's instruction. The corresponding cDNA was synthesized using a ReverTra Ace® qPCR RT Kit (cat# FSQ-101, Toyobo, Osaka, Japan). Relative expression levels of genes were measured by real-time PCR using the SYBR Green PCR Master Mix (cat# 4367659, Applied Biosystems, Waltham, MA, USA) and a StepOne™ Real-Time PCR System (Applied Biosystems). Expression levels of target genes were quantified using qRT-PCR analysis with *gapdh* detected as an internal control. The fold change of mRNA was expressed as $2^{-\Delta\Delta Ct}$. Primer pairs used for real-time PCR are listed in Appendix Table S2.

Western blot analysis

Equal amounts of protein (5~10 μg) were separated by SDS-PAGE and the transferred membranes were incubated with primary antibodies against CYP2E1 (cat# ab28146, Abcam), ADH (cat# sc-133207, Santa Cruz Biotechnology, Dallas, TX, USA), ALDH1/2 (cat# sc-

166362, Santa Cruz Biotechnology), phospho-eNOS (cat# 9570, Cell Signaling Technology), total-eNOS (cat# 32027, Cell Signaling Technology), phospho-TAK1 (cat# 9339, Cell Signaling Technology), total-TAK1 (cat# 5206, Cell Signaling Technology), phospho-JNK (cat# 4668, Cell Signaling Technology), total-JNK (cat# 9252, Cell Signaling Technology), phospho-p38 MAPK (cat# 4511, Cell Signaling Technology), total-p38 MAPK (cat# 9212, Cell Signaling Technology), phospho-ERK1/2 (cat# 4370, Cell Signaling Technology), total-ERK1/2 (cat# 4696, Cell Signaling Technology), and β-actin (cat# A5441, Sigma-Aldrich) overnight at 4°C. Immunoreactive bands were visualized using alkaline phosphatase-conjugated anti-mouse (cat# 7076, Cell Signaling Technology) or rabbit antibody (cat# 7074, Cell Signaling Technology) and the SuperSignal plus chemiluminescent substrate (cat# 34096 and 34577, Thermo Fisher Scientific). The bands were captured using an ImageSaver6 (ATTO, Tokyo, Japan) without saturation and analyzed with the CSAnalyzer 4 software (ATTO). The relative density was calculated as the ratio of the intensity of the gene of interest to that of β-actin, and all band detections were within the linear range.

Primary mouse cell isolation and treatment

Primary mouse hepatocytes, HSCs, KCs, and LSECs were isolated from *Txnip*$^{-/-}$ and WT mice as previously described (Jeong *et al*, 2011). Briefly, after collagenase perfusion of liver, the obtained cell suspension was centrifuged at 50 xg for 5 minutes at room temperature to obtain hepatocytes (pellet fraction). To purify the hepatocytes, the hepatocyte pellet was resuspended with buffer and centrifuged again at 50 xg for 5 minutes. Hepatocytes were cultured in Dulbecco′s modified Eagle′s medium (DMEM; cat# 11965-092, Gibco, Waltham, MA, USA) supplemented with 10% fetal bovine serum (FBS; Gibco) and 1% penicillin and streptomycin (Hyclone Laboratories, Logan, UT, USA) at 37°C in a humidified 5% CO_2

atmosphere. The non-parenchymal cell (NPC)-containing supernatant was centrifuged at 1,600 rpm for 10 minutes at 4°C, and the obtained cell pellet was incubated with ammonium-chloride-potassium (ACK) lysis buffer (cat# BP10-548E, Lonza, Basel, Switzerland). NPCs were separated on 11.5% and 20% Opti-Prep gradients (cat# D1556, Sigma-Aldrich) with centrifugation at 3,000 rpm for 17 minutes at 4°C for isolation of HSC and KC/LSEC fractions, respectively. Each LSEC-enriched fraction was incubated with anti-CD146 magnetic beads (cat# 130-092-007, Miltenyi Biotec, Bergisch Gladbach, Germany) and the mixture was applied to the magnetic column of a magnetic-activated cell sorting (MACS) separator. Positively selected LSECs were cultured in EGMTM-2 MV Microvascular Endothelial Cell Growth Medium-2 supplemented with an EGMTM-2 MV SingleQuots™ Supplement Pack (EBM-2; cat# CC-3202, Lonza) and 1% penicillin and streptomycin (Hyclone Laboratories) at 37°C in a humidified 5% CO_2 atmosphere. Negatively selected KCs were cultured in DMEM supplemented with 10% FBS and 1% penicillin and streptomycin at 37°C in a humidified 5% CO_2 atmosphere.

Human LSEC line

The immortalized human LSEC line, TMNK-1, was purchased from SEKISUI XenoTech (Kansas City, MO, USA). Cells were cultured in MCDB 131 (cat# 10372-019, Gibco) supplemented with an EGMTM-2 Endothelial SingleQuots™ Kit (cat# CC-4176, Lonza). To establish stable cell lines overexpressing TXNIP, TMNK-1 cells were transfected with Ctrl or TXNIP-expressing constructs (EX-M0226-Lv105 and EX-NEG-M105, GeneCopoeia, Rockville, MD, USA) using the Xfect transfection reagent (cat# 631317, Clontech Laboratories, Mountain View, CA, USA) according to the manufacturer's recommendations.

Positive clones were selected with puromycin for 3 weeks and identified using qRT-PCR and Western blotting.

In vitro ethanol or LPS experiments

For ethanol treatment, mouse primary LSECs or TMNK-1 cells were seeded on 6-well plates at 0.8~1 x 10^6 cells/mL. The cells were treated with 200 mM ethanol (cat# 459836, Sigma-Aldrich) in the culture medium for 20 hours, an additional 200 mM ethanol was added into the medium, and cultures were incubated for 4 hours. For LPS treatment, mouse primary LSECs or TMNK-1 cells were seeded on 6-well plates and treated with LPS (0.75 μg/ml; cat# L4130, Sigma-Aldrich) for the indicated time periods. For TAK1 inhibitor treatment, NG25 (500 nM; cat# S8868, Selleck Chemicals) was pre-treated for 3 hours, followed by treatment with LPS (0.75 μg/ml) for an additional 6 or 24 hours. Cells were then collected for further analyses.

MDA and total glutathione assays

Hepatic MDA and total glutathione levels were determined using a TBARS assay kit (cat# STA-330, Cell Biolabs, San Diego, CA, USA) and a total glutathione (GSSG/GSH) assay kit (cat# STA-312, Cell Biolabs), respectively, according to the manufacturers' instructions. Liver pieces were homogenized with PBS or 5% metaphosphoric acid solution and centrifuged, and supernatants were collected. The level of MDA or total glutathione was normalized based on its protein concentration or the liver weight.

ADH activity assay

ADH activity in cells was measured by a colorimetric assay kit (cat# MAK053, Sigma-Aldrich) that uses ethanol as the substrate in an enzyme reaction, according to the manufacturer's protocols. Briefly, cells were rapidly homogenized by sonication in 200 µL ice cold ADH Assay Buffer. The samples were then centrifuged at 12,000 rpm for 5 minutes. Supernatants containing equal amounts of proteins were adjusted to 50 µL final volumes with ADH Assay Buffer, combined with reaction mixes consisting of 82 µL ADH Assay Buffer, 8 µL Developer, and 10 µL 2 M ethanol, loaded to a 96-well plate, and incubated at 37°C. After 2-3 minutes, an initial measurement was taken at 450 nm. The plate was continuously incubated at 37°C and measurements were taken every 5 minutes until the value of the most active sample was greater than that of the highest standard. ADH activity was calculated by the equation provided in the manufacturer's protocol.

ALDH activity assay

ALDH activity was determined using a colorimetric assay kit (cat# MAK082, Sigma-Aldrich) according to the manufacturer's protocol. Briefly, $1x10^6$ cells were lysed by sonication in 200 µL of ice-cold ALDH Assay Buffer and centrifuged at 13,000 rpm for 5 minutes to remove insoluble material. The samples were loaded to a 96-well plate with a reaction solution consisting of 43 µL ALDH Assay Buffer, 2 µL ALDH Substrate Mix, and 5 µL acetaldehyde per well, and incubated at room temperature for 5 minutes. Colorimetric intensity was measured at 450 nm. Measurements were taken every 2-3 minutes with the plate protected from light and incubated at room temperature. The amount of NADH present in the samples was determined from the standard curve and ALDH activity was calculated by the equation provided in the manufacturer's protocol.

Determination of acetaldehyde and acetate concentrations in blood

Txnip$^{fl/fl}$ and *Txnip*$^{\Delta EC}$ mice received a single alcohol binge (5 g/kg of body weight) and blood samples were collected into heparinized tubes at 1, 2, and 3 hours after ethanol administration (n = 5 mice/time point per genotype). The acetaldehyde level was determined according to the manufacturer's protocol (cat# K-ACHYD, Megazyme, Wicklow, Ireland). After being adjusted to a 10 µL final volume, the plasma samples and standard solution were loaded to a 96-well plate. A reaction solution consisting of 200 µL distilled water, 20 µL assay buffer, and 20 µL NAD^+ was added, and samples were incubated at room temperature for approximately 2 minutes. After reading the absorbance at 340 nm, 5 µL aldehyde dehydrogenase was added into the well. The sample mixtures were incubated additionally for 4 minutes and then absorbance was measured at 340 nm. Final acetaldehyde concentration was calculated using an acetaldehyde standard solution. Acetate contents in plasma were determined according to the manufacturer's protocols (cat# MAK086, Sigma-Aldrich). Briefly, plasma samples adjusted to 50 µL final volume were loaded to a 96-well plate. A reaction solution consisting of 42 µL Acetate Assay Buffer, 2 µL Acetate Enzyme Mix, 2 µL ATP, 2 µL Acetate Substrate Mix, and 2 µL Probe was mixed with each sample and incubated at room temperature for 40 minutes. Colorimetric intensity was measured at 450 nm, and an acetate concentration was calculated using an acetate standard curve.

NO assay

Intracellular NO levels in cells were measured using Nitric Oxide Assay Kit (cat# ab219934, Abcam) according to the manufacturer's instructions. Briefly, cells were gently lifted with 0.5 mM EDTA to keep the cells intact. Cells were washed with cell culture medium and resuspended in 0.5 mL culture medium at a density of 5 x 10^5 cells/mL. Then, 1 µL 500× NO

Red Dye stock solution was added into 0.5 mL cell medium. NO formation was induced by treating stained cells with LPS and incubating them in 37ºC at 5% CO_2 incubator for 24 hours. Fluorescence increase was monitored with a flow cytometer (BD FACSCanto™ System; BD Bioscience, San Jose, CA, USA) at Ex/Em = 630/660 nm and analyzed using BD FACSDiva™ software (BD Bioscience).

IP

For IP, TAK1 plasmid was transfected into TXNIP overexpressed TMNK-1 cells and positive clones were screened with G-418 (cat# 10131035, Thermo Fisher Scientific) for 3 weeks. TAK1 cloning plasmid, pcDNA3 TAK1/F, was provided from Xin Lin (Addgene plasmid). TAK1 and TXNIP overexpressed TMNK-1 cells were lysed in cell lysis buffer (cat# 9803, Cell Signaling Technology) supplement with Phenylmethylsulfonyl fluoride (PMSF) protease inhibitor (cat# 8553, Cell Signaling Technology) as follow the manufacturer's protocols. IP was performed using Dynabead Protein A immunoprecipitation kit (cat# 10006D, Thermo Fisher Scientific). For IP test, 1-2 mg of cell lysates were immunoprecipitated with an anti-TXNIP (cat# 14715, Cell Signaling Technology), or anti-TAK antibody (cat# 5206, Cell Signaling Technology). Co-immunoprecipitated proteins were detected using western blotting with appropriate antibody.

RNA-Seq and Analysis

RNA samples were collected from LSECs isolated from *Txnip*$^{-/-}$ and WT mice. Total RNA was isolated using the TRIzol reagent (Thermo Fisher Scientific). For control and test RNAs, library construction was performed using a QuantSeq 3' mRNA-Seq Library Prep Kit (Lexogen, Vienna, Austria) according to the manufacturer's instructions. High-throughput

sequencing was performed as single-end 75 sequencing using a NextSeq 550 (Illumina, Inc., San Diego, CA, USA). QuantSeq 3' mRNA-Seq reads were aligned using Bowtie2 (Langmea d & Salzberg, 2012). DEGs were determined based on counts from unique and multiple alignments using coverage in Bedtools (Quinlan & Hall, 2010). Gene classification was based on searches done against DAVID (http://david.abcc.ncifcrf. gov/) and Medline databases (http://www.ncbi.nlm.nih.gov/). Data mining and graphic visualization were performed using ExDEGA (Ebiogen, Seoul, Korea). DEGs were identified from the criteria: log fold change > 1.3 and corrected *P* value < 0.05. Finally, a volcano map was made using the ggplot2 packet to show the differential multiples and adjusted *P* values of all genes. For hierarchical clustering analysis, the similarity between data obtained using LSECs isolated from *Txnip*$^{-/-}$ and WT mice was used to create a hierarchical nested clustering tree. The weighted average distance (weighted two-group arithmetic method, UPGMA) algorithm was adopted and the results were visualized by the HCLUST function of Rpacket. GSEA was performed to sort genes according to the degree of differential expression and detect signaling pathway changes in LSECs isolated from *Txnip*$^{-/-}$ and WT mice. The KEGG information stockpiled in the NCBI database was performed on the GSEA JAVA program; an FDR < 0.25 was considered statistically significant. The RNAseq data discussed in this publication have been deposited in NCBI's Gene Expression Omnibus and are accessible through GEO Series accession number GSE217238 (https://www.ncbi.nlm.nih.gov/geo/query/ acc.cgi?acc= GSE217238).

Statistical analysis

Data are expressed as means ± standard deviation (SD). Student's *t*-test was used to compare values between two groups. Values obtained from three or more groups were compared using

one-way analysis of variance (ANOVA) followed by Tukey's *post-hoc* test. The relationships between TXNIP expression and clinicopathological features were analyzed using the Pearson's correlation test. The incidence of hepatic tumors was evaluated with the Fisher's exact test. Statistical analysis was performed using Prism (GraphPad Software, San Diego, CA, USA). A P-value < 0.05 was considered significant.

Data availability

The datasets produced in this study are available in the following databases:

• The RNA-seq data generated in this study have been deposited at Gene Expression Omnibus (GEO) database under accession code GSE217238 (https://www.ncbi.nlm.nih.gov/geo/query/acc.cgi?acc=GSE217238).

Acknowledgements

This work was supported by the National Research Foundation of Korea (NRF) grant funded by the Korea government (MSIT) (NRF-2021R1A4A1033078 and 2022R1A2C3013064) and the Korea Research Institute of Bioscience and Biotechnology (KRIBB) Research Initiative Program (KGS1022221).

Author contributions

Eunhye Jung: Conceptualization; data curation; software; formal analysis; validation; investigation; visualization; methodology; writing–original draft; project administration. **Eun Bok Baek:** Conceptualization; data curation; software; formal analysis; validation; investigation; visualization; methodology; writing–original draft; project administration. **Eun-Ju Hong:** Formal analysis; validation; investigation; visualization; methodology. **Jee Hyun Kang:** Formal analysis; validation; investigation; visualization; methodology. **Suyoung Park:** Formal analysis; validation; investigation; visualization; methodology. **Eui-Ju Hong:** Conceptualization; resources; project administration. **Young-Eun Cho:** Conceptualization; resources; project administration. **Je-Won Ko:** Conceptualization; resources; project administration. **Young-Suk Won:** Conceptualization; resources; supervision; funding acquisition; validation; project administration; writing–review and

editing. **Hyo-Jung Kwon:** Conceptualization; resources; supervision; funding acquisition; validation; project administration; writing–review and editing.

Disclosure and competing interests statement

The authors declare that they have no conflict of interest.

The Paper Explained

Problem

Alcohol-associated liver disease (ALD) is a major cause of chronic liver disease and progress simple steatosis, steatohepatitis, fibrosis/cirrhosis and even hepatocellular carcinoma. Liver sinusoidal endothelial cells (LSECs) are highly specialized endothelial cells located the lining of the smallest blood vessels in the liver and their dysfunction promote liver disease progression. Although LSEC dysfunction are recognized as initial pathological markers in various liver diseases, including ALD, the mechanisms involved in the impact of LSECs on the development of ALD remain unclear.

Results

Here, we found that the hepatic level of thioredoxin interacting protein (TXNIP) was up-regulated in ALD patients as well as in ethanol diet-fed mice with high expression of LSECs. Notably, endothelial cell-specific *Txnip* deficiency in mice (*Txnip*$^{\Delta EC}$ mice) promoted ALD development. The increased risk of ALD in *Txnip*$^{\Delta EC}$ mice is likely due to LSEC capillarization, dysfunction, and pro-inflammatory phenotype. Mechanistically, TXNIP interacted with transforming growth factor β-activated kinase 1 (TAK1) and subsequently suppressed TAK1/c-Jun N-terminal kinase (JNK) pathway. Pharmacological inhibitor of TAK1 restored the effect of *Txnip* deficiency in LSECs, thereby blocking ethanol-induced liver injury and inflammation.

Impact

These results demonstrate that TXNIP in LSEC is a critical mediator of ALD progression through TAK1/JNK signaling and TXNIP might be a potential therapeutic target for ALD treatment.

References

Bertola A, Mathews S, Ki SH, Wang H, Gao B (2013) Mouse model of chronic and binge ethanol feeding (the NIAAA model). *Nat Protoc* 8: 627-637

Breton-Romero R, Feng B, Holbrook M, Farb MG, Fetterman JL, Linder EA, Berk BD, Masaki N, Weisbrod RM, Inagaki E *et al* (2016) Endothelial Dysfunction in Human Diabetes Is Mediated by Wnt5a-JNK Signaling. *Arterioscler Thromb Vasc Biol* 36: 561-569

Das M, Sabio G, Jiang F, Rincon M, Flavell RA, Davis RJ (2009) Induction of hepatitis by JNK-mediated expression of TNF-alpha. *Cell* 136: 249-260

Desroches-Castan A, Tillet E, Ricard N, Ouarne M, Mallet C, Belmudes L, Coute Y, Boillot O, Scoazec JY, Bailly S *et al* (2019) Bone Morphogenetic Protein 9 Is a Paracrine Factor Controlling Liver Sinusoidal Endothelial Cell Fenestration and Protecting Against Hepatic Fibrosis. *Hepatology* 70: 1392-1408

Donnelly KL, Margosian MR, Sheth SS, Lusis AJ, Parks EJ (2004) Increased lipogenesis and fatty acid reesterification contribute to hepatic triacylglycerol stores in hyperlipidemic Txnip-/- mice. *J Nutr* 134: 1475-1480

Gao B, Bataller R (2011) Alcoholic liver disease: pathogenesis and new therapeutic targets. *Gastroenterology* 141: 1572-1585

Geraud C, Koch PS, Zierow J, Klapproth K, Busch K, Olsavszky V, Leibing T, Demory A, Ulbrich F, Diett M *et al* (2017) GATA4-dependent organ-specific endothelial differentiation controls liver development and embryonic hematopoiesis. *J Clin Invest* 127: 1099-1114

Gracia-Sancho J, Caparros E, Fernandez-Iglesias A, Frances R (2021) Role of liver sinusoidal endothelial cells in liver diseases. *Nat Rev Gastroenterol Hepatol* 18: 411-431

Hammoutene A, Rautou PE (2019) Role of liver sinusoidal endothelial cells in non-alcoholic fatty liver disease. *J Hepatol* 70: 1278-1291

Hein TW, Xu X, Ren Y, Xu W, Tsai SH, Thengchaisri N, Kuo L (2019) Requisite roles of LOX-1, JNK, and arginase in diabetes-induced endothelial vasodilator dysfunction of porcine coronary arterioles. *J Mol Cell Cardiol* 131: 82-90

Hernandez-Gea V, Toffanin S, Friedman SL, Llovet JM (2013) Role of the microenvironment in the pathogenesis and treatment of hepatocellular carcinoma. *Gastroenterology* 144: 512-527

Hou X, Yang S, Yin J (2019) Blocking the REDD1/TXNIP axis ameliorates LPS-induced vascular endothelial cell injury through repressing oxidative stress and apoptosis. *Am J Physiol Cell Physiol* 316: C104-C110

Huan W, Tianzhu Z, Yu L, Shumin W (2017) Effects of Ergosterol on COPD in Mice via JAK3/STAT3/NF-kappaB Pathway. *Inflammation* 40: 884-893

Huang A, Yang YM, Yan C, Kaley G, Hintze TH, Sun D (2012) Altered MAPK signaling in progressive deterioration of endothelial function in diabetic mice. *Diabetes* 61: 3181-3188

Inokuchi S, Aoyama T, Miura K, Osterreicher CH, Kodama Y, Miyai K, Akira S, Brenner DA, Seki E (2010) Disruption of TAK1 in hepatocytes causes hepatic injury, inflammation, fibrosis, and carcinogenesis. *Proc Natl Acad Sci U S A* 107: 844-849

Jeong WI, Park O, Suh YG, Byun JS, Park SY, Choi E, Kim JK, Ko H, Wang H, Miller AM *et al* (2011) Suppression of innate immunity (natural killer cell/interferon-gamma) in the advanced stages of liver fibrosis in mice. *Hepatology* 53: 1342-1351

Junn E, Han SH, Im JY, Yang Y, Cho EW, Um HD, Kim DK, Lee KW, Han PL, Rhee SG *et al* (2000) Vitamin D3 up-regulated protein 1 mediates oxidative stress via suppressing the thioredoxin function. *J Immunol* 164: 6287-6295

Kim DO, Byun JE, Kim WS, Kim MJ, Choi JH, Kim H, Choi E, Kim TD, Yoon SR, Noh JY *et al* (2020) TXNIP Regulates Natural Killer Cell-Mediated Innate Immunity by Inhibiting IFN-gamma Production during Bacterial Infection. *Int J Mol Sci* 21

Kodama Y, Kisseleva T, Iwaisako K, Miura K, Taura K, De Minicis S, Osterreicher CH, Schnabl B, Seki E, Brenner DA (2009) c-Jun N-terminal kinase-1 from hematopoietic cells mediates progression from hepatic steatosis to steatohepatitis and fibrosis in mice. *Gastroenterology* 137: 1467-1477 e1465

Kwon HJ, Won YS, Suh HW, Jeon JH, Shao Y, Yoon SR, Chung JW, Kim TD, Kim HM, Nam KH *et al* (2010) Vitamin D3 upregulated protein 1 suppresses TNF-alpha-induced NF-kappaB activation in hepatocarcinogenesis. *J Immunol* 185: 3980-3989

Langmead B, Salzberg SL (2012) Fast gapped-read alignment with Bowtie 2. *Nat Methods* 9: 357-359

Li X, Kover KL, Heruth DP, Watkins DJ, Guo Y, Moore WV, He LG, Zang M, Clements MA, Yan Y (2017) Thioredoxin-interacting protein promotes high-glucose-induced macrovascular endothelial dysfunction. *Biochem Biophys Res Commun* 493: 291-297

Li X, Rong Y, Zhang M, Wang XL, LeMaire SA, Coselli JS, Zhang Y, Shen YH (2009) Up-regulation of thioredoxin interacting protein (Txnip) by p38 MAPK and FOXO1 contributes to the impaired thioredoxin activity and increased ROS in glucose-treated endothelial cells. *Biochem Biophys Res Commun* 381: 660-665

Liu Y, Wang Y, Miao X, Zhou S, Tan Y, Liang G, Zheng Y, Liu Q, Sun J, Cai L (2014) Inhibition of JNK by compound C66 prevents pathological changes of the aorta in STZ-induced diabetes. *J Cell Mol Med* 18: 1203-1212

Mahata T, Sengar AS, Basak M, Das K, Pramanick A, Verma SK, Singh PK, Biswas S, Sarkar S, Saha S *et al* (2021) Hepatic Regulator of G Protein Signaling 6 (RGS6) drives non-alcoholic fatty liver disease by promoting oxidative stress and ATM-dependent cell death. *Redox Biol* 46: 102105

Mak KM, Kee D, Shin DW (2022) Alcohol-associated capillarization of sinusoids: A critique since the discovery by Schaffner and Popper in 1963. *Anat Rec (Hoboken)* 305: 1592-1610

Marrone G, Russo L, Rosado E, Hide D, Garcia-Cardena G, Garcia-Pagan JC, Bosch J, Gracia-Sancho J (2013) The transcription factor KLF2 mediates hepatic endothelial protection and paracrine endothelial-stellate cell deactivation induced by statins. *J Hepatol* 58: 98-103

McCuskey RS, Bethea NW, Wong J, McCuskey MK, Abril ER, Wang X, Ito Y, DeLeve LD (2005) Ethanol binging exacerbates sinusoidal endothelial and parenchymal injury elicited by acetaminophen. *J Hepatol* 42: 371-377

Mohamed IN, Li L, Ismael S, Ishrat T, El-Remessy AB (2021) Thioredoxin interacting protein, a key molecular switch between oxidative stress and sterile inflammation in cellular response. *World J Diabetes* 12: 1979-1999

Nishiyama A, Matsui M, Iwata S, Hirota K, Masutani H, Nakamura H, Takagi Y, Sono H, Gon Y, Yodoi J (1999) Identification of thioredoxin-binding protein-2/vitamin D(3) up-regulated protein 1 as a negative regulator of thioredoxin function and expression. *J Biol Chem* 274: 21645-21650

Osna NA, Donohue TM, Jr., Kharbanda KK (2017) Alcoholic Liver Disease: Pathogenesis and Current Management. *Alcohol Res* 38: 147-161

Pan M, Zhang F, Qu K, Liu C, Zhang J (2022) TXNIP: A Double-Edged Sword in Disease and Therapeutic Outlook. *Oxid Med Cell Longev* 2022: 7805115

Park HS, Song JW, Park JH, Lim BK, Moon OS, Son HY, Lee JH, Gao B, Won YS, Kwon HJ (2021) TXNIP/VDUP1 attenuates steatohepatitis via autophagy and fatty acid oxidation. *Autophagy* 17: 2549-2564

Park MJ, Kim DI, Lim SK, Choi JH, Kim JC, Yoon KC, Lee JB, Lee JH, Han HJ, Choi IP *et al* (2014) Thioredoxin-interacting protein mediates hepatic lipogenesis and inflammation via PRMT1 and PGC-1alpha regulation in vitro and in vivo. *J Hepatol* 61: 1151-1157

Pham PT, Fukuda D, Yagi S, Kusunose K, Yamada H, Soeki T, Shimabukuro M, Sata M (2019) Rivaroxaban, a specific FXa inhibitor, improved endothelium-dependent relaxation of aortic segments in diabetic mice. *Sci Rep* 9: 11206

Poisson J, Lemoinne S, Boulanger C, Durand F, Moreau R, Valla D, Rautou PE (2017) Liver sinusoidal endothelial cells: Physiology and role in liver diseases. *J Hepatol* 66: 212-227

Qian Q, Li Y, Fu J, Leng D, Dong Z, Shi J, Shi H, Cao D, Cheng X, Hu Y *et al* (2022) Switch-associated protein 70 protects against nonalcoholic fatty liver disease through suppression of TAK1. *Hepatology* 75: 1507-1522

Quinlan AR, Hall IM (2010) BEDTools: a flexible suite of utilities for comparing genomic features. *Bioinformatics* 26: 841-842

Schattenberg JM, Singh R, Wang Y, Lefkowitch JH, Rigoli RM, Scherer PE, Czaja MJ (2006) JNK1 but not JNK2 promotes the development of steatohepatitis in mice. *Hepatology* 43: 163-172

Schulze PC, Liu H, Choe E, Yoshioka J, Shalev A, Bloch KD, Lee RT (2006) Nitric oxide-dependent suppression of thioredoxin-interacting protein expression enhances thioredoxin activity. *Arterioscler Thromb Vasc Biol* 26: 2666-2672

Tan S, Zhao J, Sun Z, Cao S, Niu K, Zhong Y, Wang H, Shi L, Pan H, Hu J *et al* (2020) Hepatocyte-specific TAK1 deficiency drives RIPK1 kinase-dependent inflammation to promote liver fibrosis and hepatocellular carcinoma. *Proc Natl Acad Sci U S A* 117: 14231-14242

Tateya S, Rizzo NO, Handa P, Cheng AM, Morgan-Stevenson V, Daum G, Clowes AW, Morton GJ, Schwartz MW, Kim F (2011) Endothelial NO/cGMP/VASP signaling attenuates Kupffer cell activation and hepatic insulin resistance induced by high-fat feeding. *Diabetes* 60: 2792-2801

Urashima S, Tsutsumi M, Nakase K, Wang JS, Takada A (1993) Studies on capillarization of the hepatic sinusoids in alcoholic liver disease. *Alcohol Alcohol Suppl* 1B: 77-84

Wang R, Guo Y, Li L, Luo M, Peng L, Lv D, Cheng Z, Xue Q, Wang L, Huang J (2022) Role of thioredoxin-interacting protein in mediating endothelial dysfunction in hypertension. *Genes Dis* 9: 753-765

Wang XQ, Nigro P, World C, Fujiwara K, Yan C, Berk BC (2012) Thioredoxin interacting protein promotes endothelial cell inflammation in response to disturbed flow by increasing leukocyte adhesion and repressing Kruppel-like factor 2. *Circ Res* 110: 560-568

Wilkinson AL, Qurashi M, Shetty S (2020) The Role of Sinusoidal Endothelial Cells in the Axis of Inflammation and Cancer Within the Liver. *Front Physiol* 11: 990

Xie G, Wang X, Wang L, Wang L, Atkinson RD, Kanel GC, Gaarde WA, Deleve LD (2012) Role of differentiation of liver sinusoidal endothelial cells in progression and regression of hepatic fibrosis in rats. *Gastroenterology* 142: 918-927 e916

Yang Y, Sangwung P, Kondo R, Jung Y, McConnell MJ, Jeong J, Utsumi T, Sessa WC, Iwakiri Y (2021) Alcohol-induced Hsp90 acetylation is a novel driver of liver sinusoidal endothelial dysfunction and alcohol-related liver disease. *J Hepatol* 75: 377-386

Zakhari S (2006) Overview: how is alcohol metabolized by the body? *Alcohol Res Health* 29: 245-254

Zhang JK, Ding MJ, Liu H, Shi JH, Wang ZH, Wen PH, Zhang Y, Yan B, Guo DF, Zhang XD *et al* (2022) Regulator of G-protein signaling 14 protects the liver from ischemia-reperfusion injury by suppressing TGF-beta-activated kinase 1 activation. *Hepatology* 75: 338-352

Zhao S, Zhang Z, Yao Z, Shao J, Chen A, Zhang F, Zheng S (2017) Tetramethylpyrazine attenuates sinusoidal angiogenesis via inhibition of hedgehog signaling in liver fibrosis. *IUBMB Life* 69: 115-127

Figure legends

Figure 1. TXNIP expression is increased in liver tissues of ALD patients and ethanol-diet fed mice.

A. Representative images of immunohistochemical staining for TXNIP in liver sections from normal controls (n = 13), alcohol-associated steatosis patients (n = 19), and alcohol-associated fibrosis patients (n = 18). Original magnification = X400. The integrated optical density (IOD) of TXNIP-positive areas is shown on the right.

B. Association between TXNIP expression and macro-fat or alcohol consumption in normal controls and ALD patients.

C. Correlation between TXNIP expression and fibrosis grade or alcohol consumption.

D. Representative immunohistochemical images of TXNIP expression in mice fed a control or 4% ethanol diet for 1-year (n = 4). Scale bars, 50 μM. The IOD of TXNIP-positive areas is shown on the right.

E. Hepatic expression of *TXNIP* mRNA in mice fed a control or 4% ethanol diet for 1 year (n = 4).

Data information: All data are shown as means ± SD. Data were analyzed by one-way ANOVA with Tukey's multiple comparisons test (A), Pearson's correlation test (B, C), and unpaired Student's t-test (D, E). "ns" stands for "not significant."

Figure 2. A lack of *Txnip* increases ethanol-induced hepatocarcinogenesis.

A-F. *Txnip*$^{-/-}$ and WT mice were fed a control or 4% ethanol diet for 1 year. (A) Survival rate after 1 year of ethanol treatment (pair-fed WT, n = 8; pair-fed *Txnip*$^{-/-}$, n = 8; EtOH WT, n = 16; EtOH *Txnip*$^{-/-}$, n = 16). (B) Serum levels of ALT and AST (pair-fed WT, n = 5; pair-fed *Txnip*$^{-/-}$, n = 3; EtOH WT, n = 15; EtOH *Txnip*$^{-/-}$, n = 9). (C) The incidence and maximum

size of tumor after ethanol feeding (WT, n = 15; *Txnip*$^{-/-}$, n = 9). (D) Representative gross findings of livers. Arrow indicates liver tumor. (E) H&E staining of livers at low (scale bars, 50 μM) and high (scale bars, 100 μM) magnification. Note the tumor (arrows) compressing adjacent normal liver tissue in *Txnip*$^{-/-}$ mice. (F) Representative Oil red O staining, Sirius red staining, and immunohistochemistry of F4/80 and MPO (n = 3). Scale bars, 50 μM or 100 μM. Data information: All data are shown as means ± SD. Data were analyzed by Long-rank (Mantel-Cox) test (A), two-way ANOVA (B, F), Fisher's exact test, and unpaired Student's t-test (C). "ns" stands for "not significant."

Figure 3. A deficiency of *Txnip* in LSECs increases ethanol-induced hepatocarcinogenesis.

A. Relative mRNA levels of TXNIP. Hepatocytes, KCs, and LSECs were isolated form *Txnip*$^{-/-}$ and WT mice after 10 day plus gavage (pair-fed, n = 4; EtOH, n = 6).

B. Immunofluorescence staining of WT mice. Note the co-localization of TXNIP and F4/80 or LYVE-1 (arrows). Original magnification = X400.

C. Validation of KCs and LSECs TXNIP deletion in *Txnip*$^{\Delta Mac}$ and *Txnip*$^{\Delta EC}$ mice. KCs and LSECs were isolated from *Txnip*$^{fl/fl}$, *Txnip*$^{\Delta Mac}$, and *Txnip*$^{\Delta EC}$ mice (n = 3).

D-G. *Txnip*$^{fl/fl}$, *Txnip*$^{\Delta Mac}$, and *Txnip*$^{\Delta EC}$ mice by crossing were fed a 5% ethanol diet for 4 weeks and analyzed for serum ALT and AST (D), hepatic triglyceride and cholesterol (E), relative hepatic mRNA levels of inflammatory response genes (F), and the levels of MDA and total glutathione (G) (n = 6).

H-J. *Txnip*$^{fl/fl}$ and *Txnip*$^{\Delta EC}$ mice were fed a liquid control diet or 4% ethanol diet for 1 year. Representative gross findings and H&E staining of livers (H), the incidence and maximum size of tumors (I), and serum levels of ALT and AST (J) (*Txnip*$^{fl/fl}$, n = 16; *Txnip*$^{\Delta EC}$, n =5).

Note tumor nodule (arrows) compressing adjacent normal liver tissue in *Txnip*$^{\Delta EC}$ mice. Scale bars, 200 μM.

Data information: All data are shown as means ± SD. Data were analyzed by two-way ANOVA (A), unpaired Student's t-test (A, C, I, J), one-way ANOVA (D-G), and Fisher's exact test (I). "ns" stands for "not significant."

Figure 4. TXNIP regulates LSEC phenotype and function.

A. GSEA of RNA-seq data from LSECs of *Txnip*$^{-/-}$ and WT mice (n = 3). The 20 most significantly enriched pathways are shown.

B. Relative mRNA levels of LSECs and capillary EC markers (n = 4). LSECs isolated form *Txnip*$^{-/-}$ and WT mice treated with LPS (0.75 μg/ml) for 6 hours.

C. Immunofluorescence staining of LYVE-1 and CD31 (n = 5). *Txnip*$^{fl/fl}$ and *Txnip*$^{\Delta EC}$ mice were fed a control or 4% ethanol diet for 1 year. LYVE-1- or CD31-positive areas are shown on the right. Original magnification = X400.

D-G. LSECs isolated from *Txnip*$^{-/-}$ and WT mice were incubated with LPS (0.75 μg/ml for 6 hours) and subjected to Western blotting (D) (n = 4), RT-qPCR analysis (E and G) (n = 4), and NO assay (F) (n = 3).

Data information: All data are shown as means ± SD. Data were analyzed by unpaired Student's t-test (A) and two-way ANOVA (B, C, D, E, F, G). "ns" stands for "not significant."

Fig. 5. TXNIP is involved in alcohol metabolism of LSECs.

A. Volcano map showing DGEs in LSECs isolated from *Txnip*$^{-/-}$ and WT mice (n = 3).

B. The top 10 most significantly enriched pathways contributing to TXNIP function based on KEGG enrichment analysis.

C, D. LSECs isolated from *Txnip*$^{-/-}$ and WT mice were incubated with ethanol (200 mM) for 24 hours and subjected to ELISA (C) (n = 3) and Western blotting (D) (n = 4).

E, F. *Txnip*$^{fl/fl}$ and *Txnip*$^{\Delta EC}$ mice received a single alcohol binge (5 g/kg of body weight) and subjected to immunoblot analysis (E) and ELISA (F) (n = 5).

Data information: All data are shown as means ± SD. Data were analyzed by unpaired Student's t-test (A) and two-way ANOVA (C, D, E, F). "ns" stands for "not significant."

Figure. 6. TXNIP inhibits TAK1/JNK signaling in LSECs.

A. Protein expression of TAK1 and JNK. LSECs isolated from *Txnip*$^{-/-}$ and WT mice were incubated with LPS (0.75 μg/ml) for 30 minutes (n = 4).

B. Immunoblot analysis (n = 4 biological replicates). Control and TXNIP-overexpressed TMNK-1 cells were incubated with LPS (0.75 μg/ml) for 30 minutes.

C. Western blot analysis of liver tissues (pair-fed, n = 3; EtOH, n = 4). *Txnip*$^{fl/fl}$ and *Txnip*$^{\Delta EC}$ mice were fed a control or 4% ethanol diet for 1 year.

D. Immunofluorescence staining of TXNIP and TAK1 in TMNK-1 cells.

E. Representative co-IP analysis of TXNIP and TAK1 in TMNK-1 cells.

Data information: All data are shown as means ± SD. Data were analyzed by two-way ANOVA. "ns" stands for "not significant."

Figure 7. TAK1 inhibition blocks ethanol-induced liver injury, oxidative stress, and inflammation caused by *Txnip* deficiency in LSECs.

A-C. LSECs isolated from *Txnip*$^{-/-}$ and WT mice were incubated with NG25 (500 nM) for 3 hours, incubated with LPS (0.75 μg/ml) for 0.5 or 6 hours, and subjected to Western blotting (A) and RT-qPCR analysis (B, C) (n = 4).

D-G. *Txnip*$^{fl/fl}$ and *Txnip*$^{\Delta EC}$ mice were fed a 5% ethanol diet with NG25 (5 mg/kg/day) for 4 weeks and subjected to H&E staining (D), blood chemistry analysis (E), oxidative stress analysis (F), and RT-qPCR analysis (G) (n = 5).

Data information: All data are shown as means ± SD. Data were analyzed by two-way ANOVA. "ns" stands for "not significant."

Figure 8. Positive correlation between hepatic TXNIP expression and LSEC capillarization in ALD patients.

A. Representative images of immunohistochemical staining for LYVE-1 and CD31 in liver sections from normal controls (n = 12) and alcohol-associated fibrosis patients (n = 17). Scale bars, 50 μM.

B. LYVE-1- and CD31-positive areas.

C. Negative correlation of hepatic LYVE-1 expression and fibrosis grade or alcohol consumption.

D. Positive association of hepatic CD31 expression and fibrosis grade or alcohol consumption.

E. Immunofluorescence staining of liver sections. Note the co-localization of TXNIP and LYVE-1 or CD31 (arrows). Original magnification = X400.

F. Immunohistochemical images of TXNIP expression. Note the TXNIP-positive LSECs (arrows) in human liver tissues. Scale bars, 30 μM.

G. Correlation of TXNIP expression and LYVE-1- or CD31-positive area in normal and ALD patients.

Data information: All data are shown as means ± SD. Data were analyzed by unpaired Student's t-test (B) and Pearson's correlation test (C, D, G). "ns" stands for "not significant."

Jung *et al.*, Fig. 1

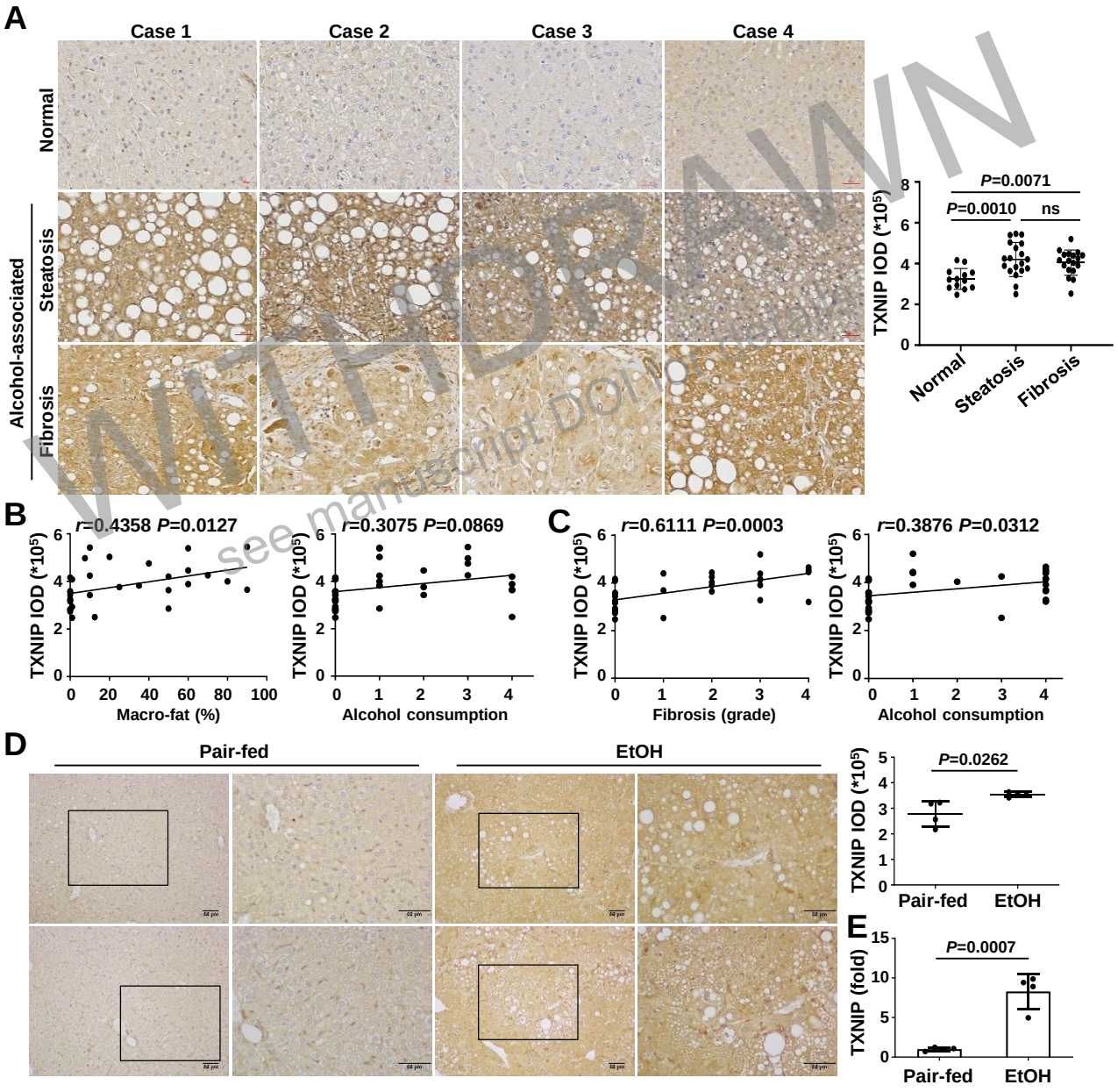

Jung *et al.*, Fig. 2

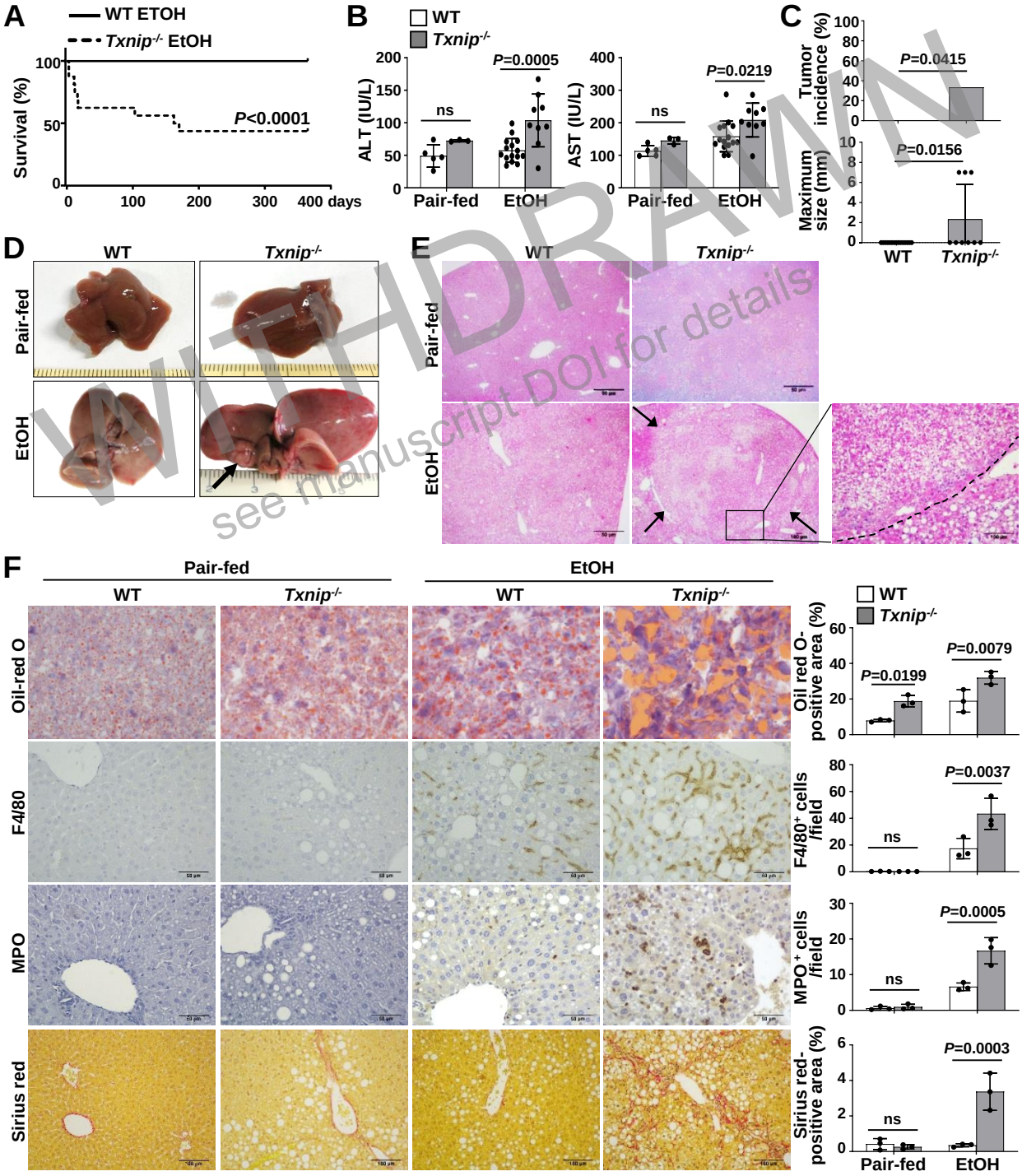

Jung *et al.*, Fig. 3

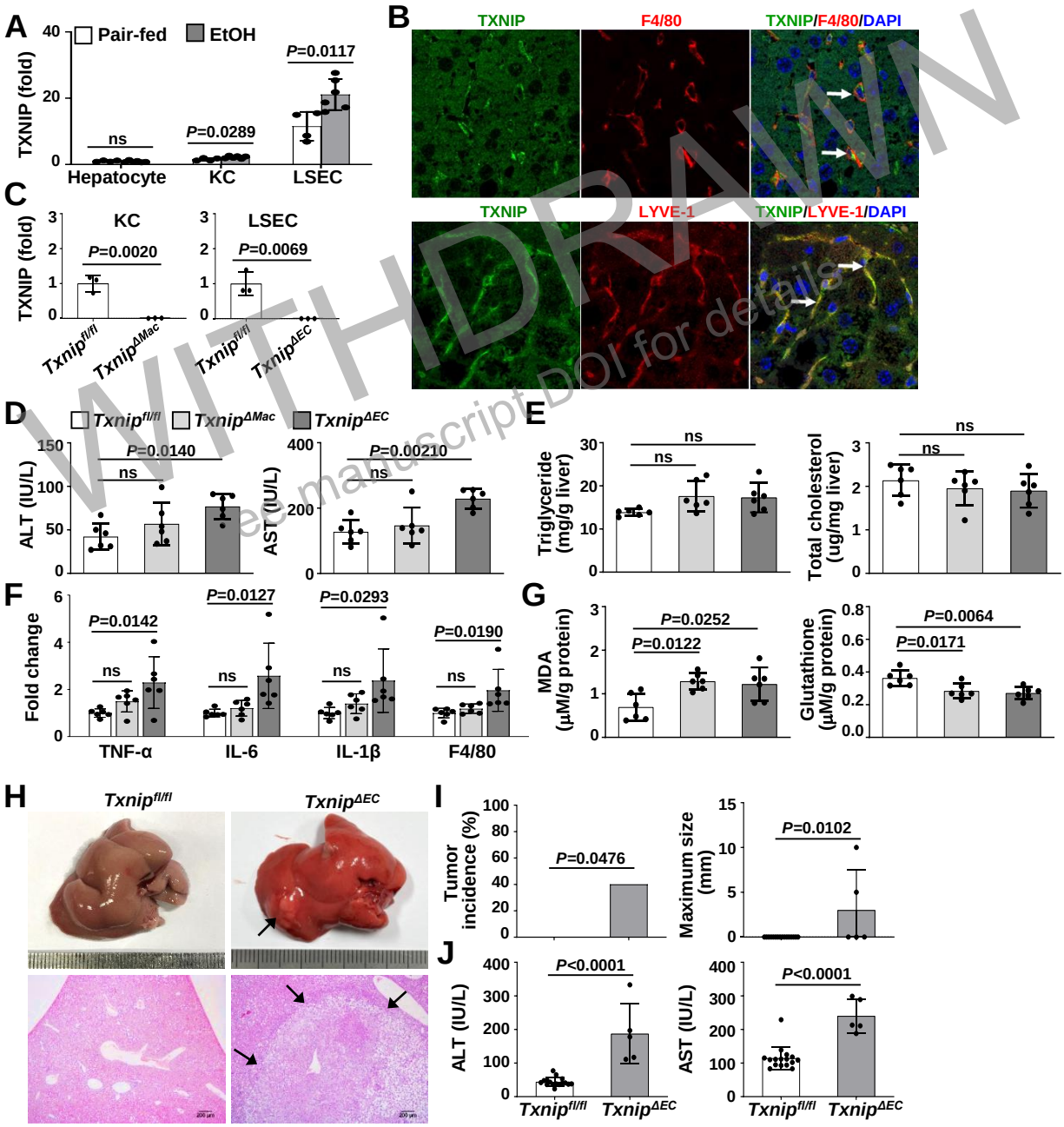

Jung *et al.*, Fig. 4

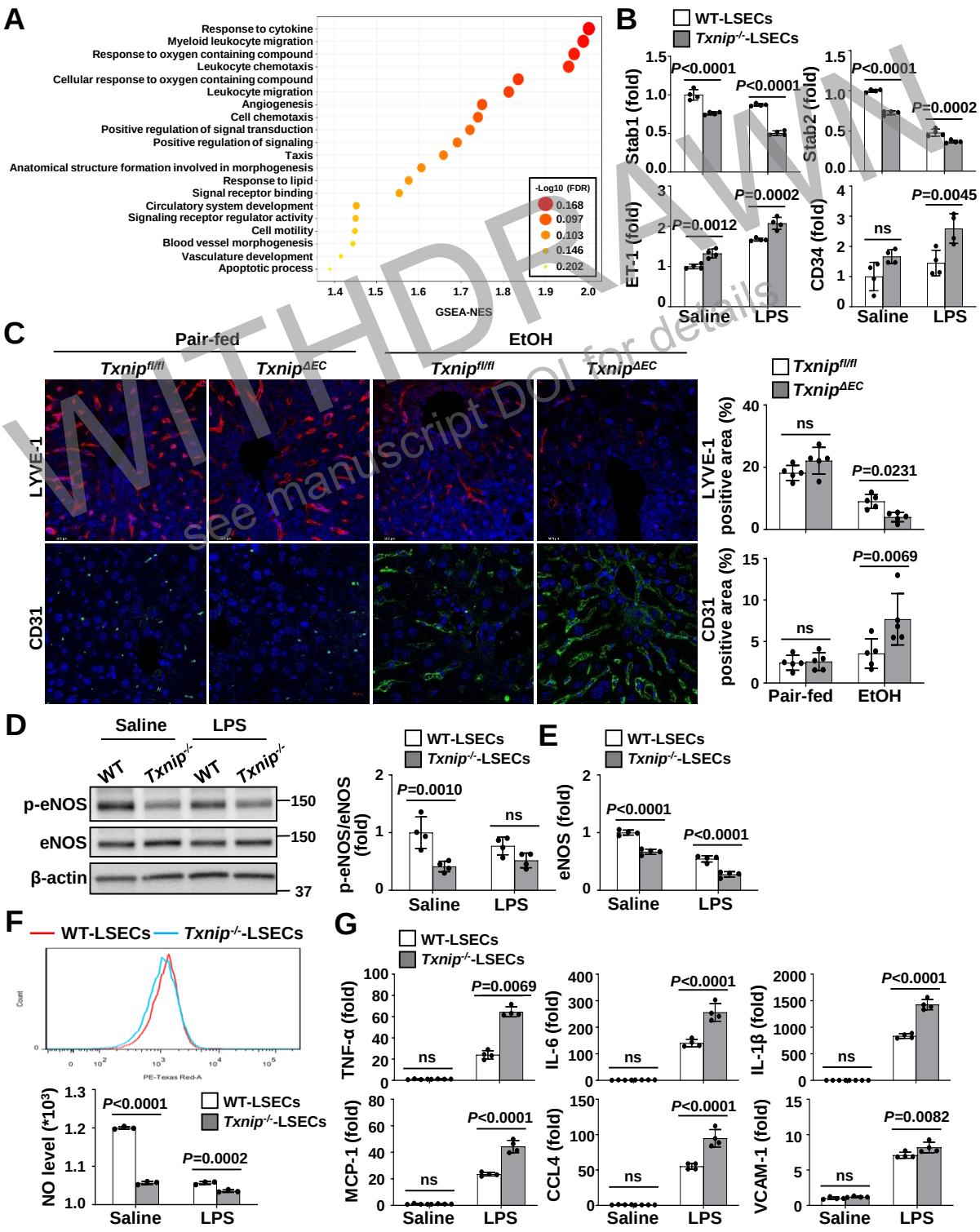

Jung *et al.*, Fig. 5

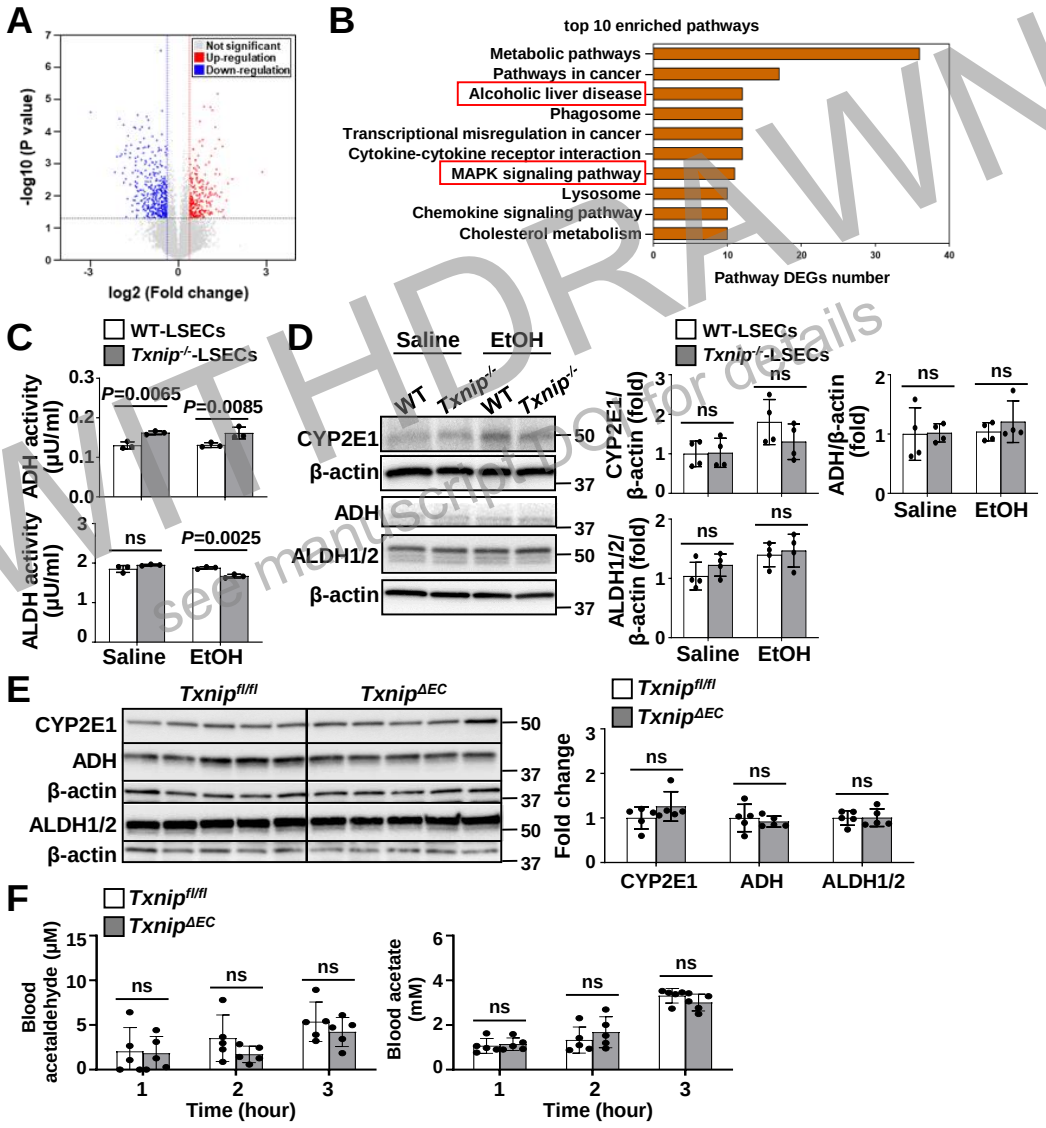

Jung *et al.*, Fig. 6

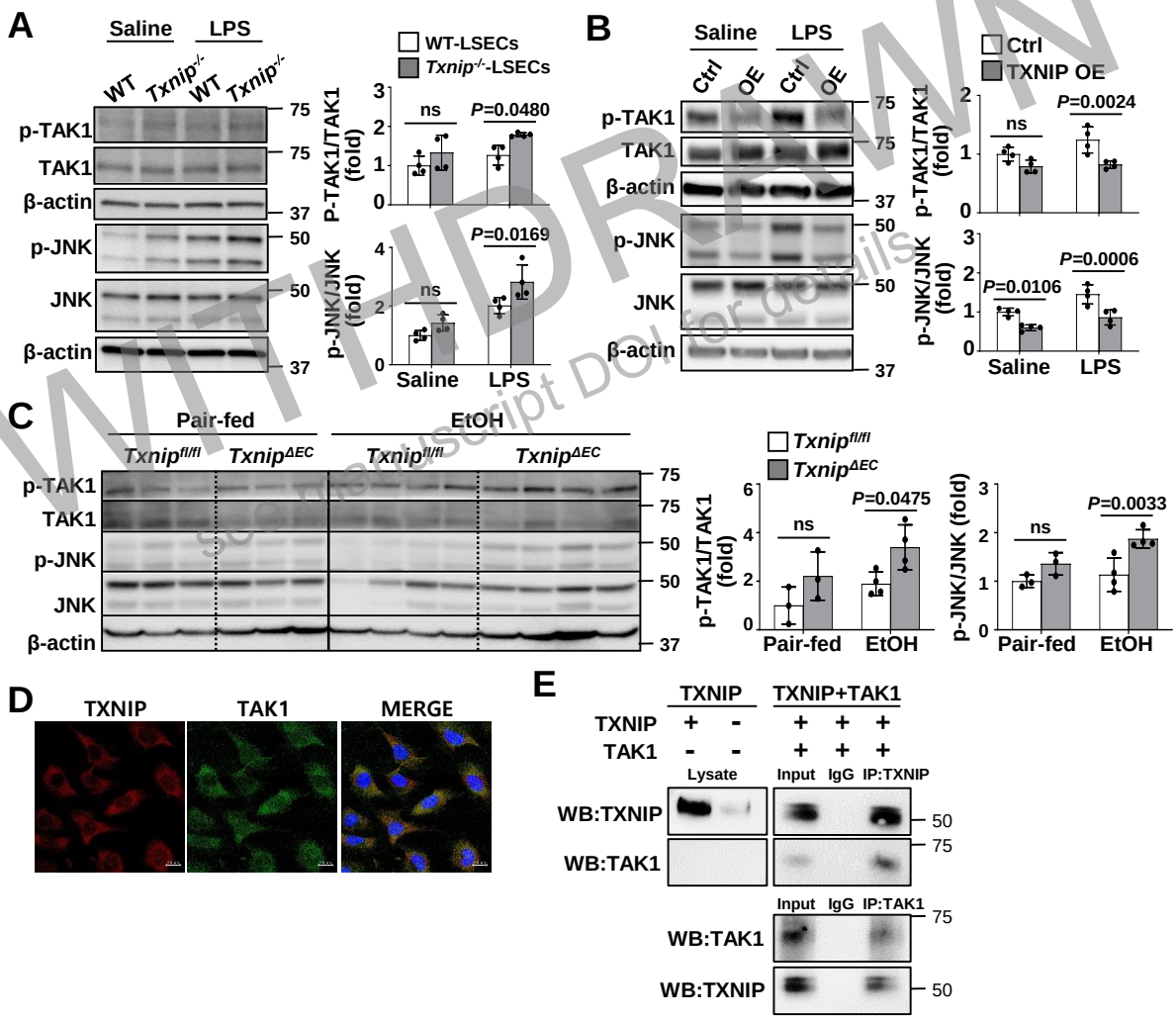

Jung *et al.*, Fig. 7

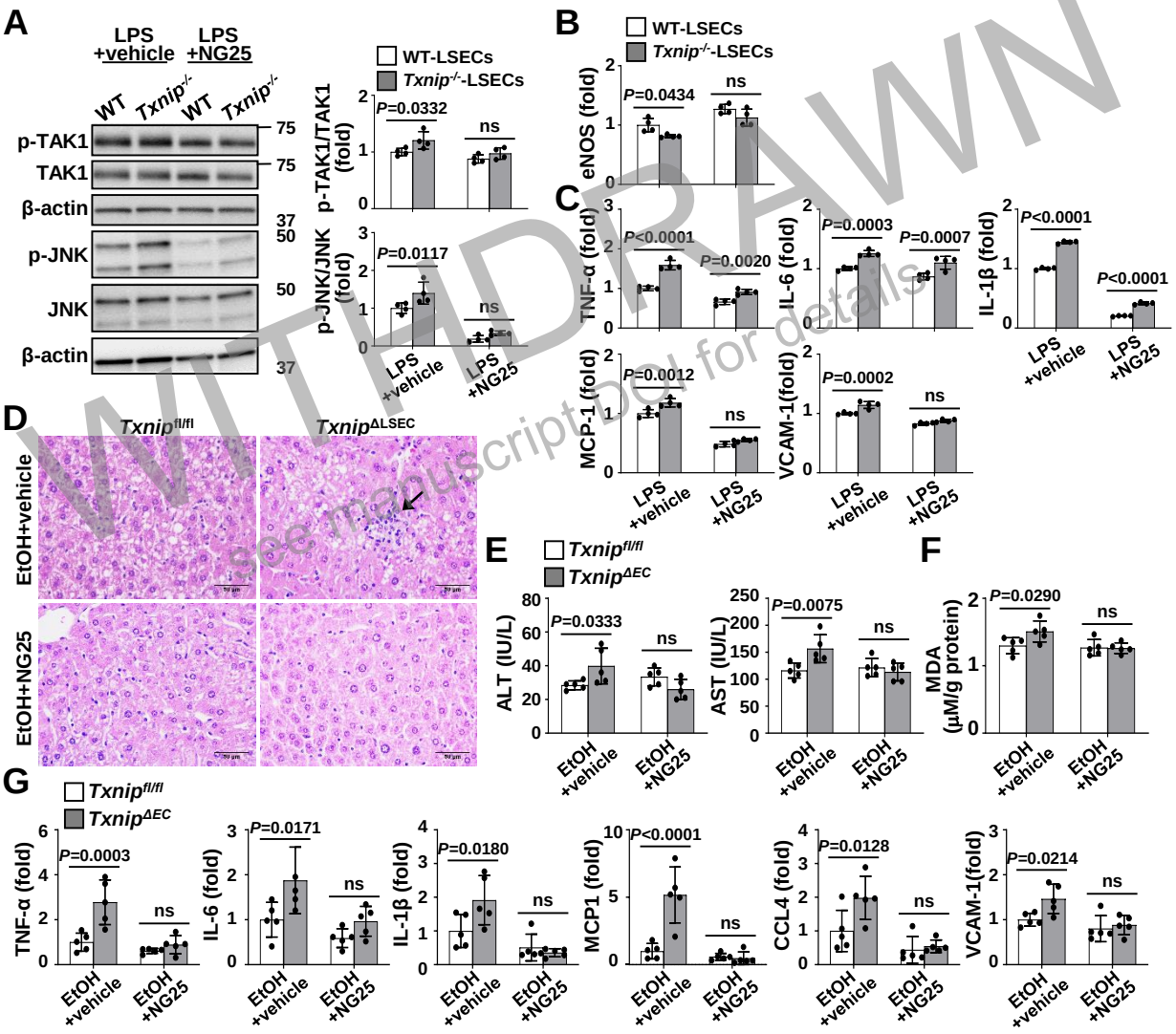

Jung *et al.*, Fig. 8